



Improved measurement of η/η' mixing in $B_{(s)}^0 \rightarrow J/\psi\eta^{(\prime)}$ decays

 LHCb collaboration[†]

Abstract

Branching fraction ratios between the decays $B_{(s)}^0 \rightarrow J/\psi\eta^{(\prime)}$ are measured using proton-proton collision data collected by the LHCb experiment at centre-of-mass energies of 7, 8 and 13 TeV, corresponding to an integrated luminosity of 9 fb^{-1} . The measured ratios of these branching fractions are

$$\frac{\mathcal{B}(B^0 \rightarrow J/\psi\eta')}{\mathcal{B}(B^0 \rightarrow J/\psi\eta)} = 0.48 \pm 0.06 \pm 0.02 \pm 0.01,$$

$$\frac{\mathcal{B}(B_s^0 \rightarrow J/\psi\eta')}{\mathcal{B}(B_s^0 \rightarrow J/\psi\eta)} = 0.80 \pm 0.02 \pm 0.02 \pm 0.01,$$

where the uncertainties are statistical, systematic and related to the precision of the $\eta^{(\prime)}$ branching fractions, respectively. They are used to constrain the η/η' mixing angle, ϕ_P , and to probe the presence of a possible glueball component in the η' meson, described by the gluonic mixing angle ϕ_G . The obtained results are

$$\phi_P = (41.6_{-1.2}^{+1.0})^\circ,$$

$$\phi_G = (28.1_{-4.0}^{+3.9})^\circ,$$

where the uncertainties are statistically dominated. While the value of ϕ_P is compatible with existing experimental determinations and theoretical calculations, the angle ϕ_G differs from zero by more than four standard deviations, which points to a substantial glueball component in the η' meson and/or unexpectedly large contributions from gluon-mediated processes in these decays. The absolute branching fractions are also measured relative to that of the well-established $B_s^0 \rightarrow J/\psi\phi$ decay, which serves as the normalisation channel. These results supersede the previous LHCb measurements and are the most precise to date.

Submitted to JHEP

 © 2025 CERN for the benefit of the LHCb collaboration. [CC BY 4.0 licence](#).

[†]Authors are listed at the end of this paper.

1 Introduction

Decays of the $\eta^{(\prime)}$ mesons provide a unique, flavour-conserving laboratory to test low-energy quantum chromodynamics (QCD) and search for physics beyond the Standard Model [1]. Their properties reflect the low-energy dynamics of quarks and gluons — the fundamental degrees of freedom of QCD — and remain challenging to predict due to the effects of confinement. The constituent quark model [2] describes the η and η' pseudoscalar mesons as linear combinations of the isospin-0 octet and singlet SU(3)-flavour states, where mixing is a consequence of the larger mass of the s quark relative to the u and d quarks. These combinations are parametrised by a mixing angle, whose predicted value lies between -25° and -10° , defining the η' (η) meson as mostly singlet (octet) state.

More elaborate approaches to calculate the properties of light hadrons rely on the symmetry properties of QCD, such as the approximate chiral symmetry among light quarks [3]. This spontaneously broken symmetry generates the octet of pseudoscalar mesons and forms the basis for chiral perturbation theory (χ PT) [4]. In the large-number-of-colours limit of QCD, χ PT can be extended to include the singlet state, providing a consistent framework to describe the mixing parameters, and showing that a one-angle description is only valid at leading order in perturbation theory [5,6].

Phenomenological analyses of different physics processes, such as transitions between light and heavy hadrons (*e.g.* $D_s^+ \rightarrow \eta^{(\prime)} e^+ \nu_e$,¹ $V \rightarrow \eta^{(\prime)} \gamma$ with $V = J/\psi, \phi$), diphoton decays (*e.g.* $\eta^{(\prime)} \rightarrow \gamma\gamma$) and annihilation processes (*e.g.* $p\bar{p} \rightarrow PM$ with P a pseudoscalar meson and $M = \pi^0, \eta, \omega$) [7–9], advocate the use of two angles to describe η/η' mixing in the octet/singlet basis. These analyses also emphasise the special role of the quark basis, spanned by the states $|\eta_q\rangle = 1/\sqrt{2}(|u\bar{u}\rangle + |d\bar{d}\rangle)$ and $|\eta_s\rangle = |s\bar{s}\rangle$, where these two angles take compatible values and are replaced by a single angle, ϕ_P , with a value of around 40° (see Ref. [10] for a review of recent determinations). First-principle calculations on the lattice are becoming competitive in precision and agree with these determinations [11–13]. Possible $\eta^{(\prime)}$ mixing with π^0 mesons or charmonium has also been investigated and found to be negligible [7,14].

Another intriguing aspect of $\eta^{(\prime)}$ mesons is their possible gluonic content and the connection with glueballs, the colour singlet states made of two or more gluons predicted by QCD [15]. Interestingly, the QCD anomaly [16–18] contributes to the singlet mass by a purely gluonic component which, due to mixing, mostly affects the η' meson [19]. Because of its gluonic content, the η' meson may mix with glueballs [20,21], hence changing the rates of physics processes where it is involved (*e.g.* $B^+ \rightarrow K^+ \eta'$ [22], $B_{(s)}^0 \rightarrow J/\psi \eta'$ [23]), and providing indirect constraints on the mass of the lightest pseudoscalar glueball [24]. Current experimental results suggest a negligible glueball component in the η' meson, although earlier reports indicated potentially large contributions with limited statistical significance [8,22,25–28]. Potential glueball components to the η meson have also been investigated using J/ψ decays [26] and were not found to be significant.

At the quark level, $B_{(s)}^0 \rightarrow J/\psi \eta^{(\prime)}$ decays proceed dominantly through the tree-level transition $b \rightarrow c\bar{c}q$, where q is either a d or an s quark that forms an $\eta^{(\prime)}$ meson with the spectator quark. Neglecting decay topologies where the spectator quark participates in the flavour-changing interaction and the $\eta^{(\prime)}$ or J/ψ meson is produced by gluons, simple relations between decay amplitudes can be derived which relate the relative decay rates to

¹Inclusion of charge-conjugate processes is implied throughout.

the mixing angle ϕ_P [29]. These relations allow to test the validity of the one-angle η/η' mixing scheme (standard mixing) or the presence of the aforementioned gluon-mediated processes coupling differently to the two mesons. As proposed in Ref. [23], the standard mixing scheme can be extended to incorporate a glueball component to the η' wave function. In the quark basis, the physical states are written as

$$\begin{aligned} |\eta\rangle &= \cos\phi_P |\eta_q\rangle - \sin\phi_P |\eta_s\rangle, \\ |\eta'\rangle &= \cos\phi_G (\sin\phi_P |\eta_q\rangle + \cos\phi_P |\eta_s\rangle) + \sin\phi_G |gg\rangle, \end{aligned} \quad (1)$$

where $|gg\rangle$ denotes a glueball state and ϕ_G is the gluonic angle. Projecting out the physical states to the basis states, the following relations between branching fractions are obtained:

$$R_d \equiv \frac{\mathcal{B}(B^0 \rightarrow J/\psi\eta')}{\mathcal{B}(B^0 \rightarrow J/\psi\eta)} \cdot \frac{\Phi^3(B^0 \rightarrow J/\psi\eta)}{\Phi^3(B^0 \rightarrow J/\psi\eta')} = \tan^2\phi_P \cdot \cos^2\phi_G, \quad (2)$$

$$R_s \equiv \frac{\mathcal{B}(B_s^0 \rightarrow J/\psi\eta')}{\mathcal{B}(B_s^0 \rightarrow J/\psi\eta)} \cdot \frac{\Phi^3(B_s^0 \rightarrow J/\psi\eta)}{\Phi^3(B_s^0 \rightarrow J/\psi\eta')} = \cot^2\phi_P \cdot \cos^2\phi_G, \quad (3)$$

where the Φ terms are phase-space factors defined as

$$\Phi(B_{(s)}^0 \rightarrow J/\psi\eta^{(\prime)}) = \sqrt{\left[1 - \left(\frac{m_{J/\psi} - m_{\eta^{(\prime)}}}{m_{B_{(s)}^0}}\right)^2\right] \left[1 - \left(\frac{m_{J/\psi} + m_{\eta^{(\prime)}}}{m_{B_{(s)}^0}}\right)^2\right]}, \quad (4)$$

that are raised to the power three in Eqs. 2 and 3 to account for the spin configuration of the decay. The values for the angles can then be obtained from a combination of the $R_{d,s}$ ratios, as

$$\tan^4\phi_P = R_d / R_s, \quad (5)$$

$$\cos^4\phi_G = R_d \cdot R_s, \quad (6)$$

where, in the case of standard mixing, $\phi_G = 0$ and $R_d \cdot R_s = 1$ [29]. Similarly, one can calculate the following ratios which only depend on ϕ_P ,

$$R_\eta \equiv \frac{\mathcal{B}(B^0 \rightarrow J/\psi\eta)}{\mathcal{B}(B_s^0 \rightarrow J/\psi\eta)} \cdot \frac{\Phi^3(B_s^0 \rightarrow J/\psi\eta)}{\Phi^3(B^0 \rightarrow J/\psi\eta)} = \frac{\tau_{B^0} m_{B^0}}{\tau_{B_s^0} m_{B_s^0}} \left| \frac{V_{cd}}{V_{cs}} \right|^2 \frac{\cot^2\phi_P}{2}, \quad (7)$$

$$R_{\eta'} \equiv \frac{\mathcal{B}(B^0 \rightarrow J/\psi\eta')}{\mathcal{B}(B_s^0 \rightarrow J/\psi\eta')} \cdot \frac{\Phi^3(B_s^0 \rightarrow J/\psi\eta')}{\Phi^3(B^0 \rightarrow J/\psi\eta')} = \frac{\tau_{B^0} m_{B^0}}{\tau_{B_s^0} m_{B_s^0}} \left| \frac{V_{cd}}{V_{cs}} \right|^2 \frac{\tan^2\phi_P}{2}, \quad (8)$$

which hold up to SU(3)-breaking corrections, and where m , τ and V_{ij} are the $B_{(s)}^0$ mass and lifetime, and CKM matrix elements, respectively [29].

Initial experimental results were reported in 2012 by the Belle collaboration for the decay $B^0 \rightarrow J/\psi\eta$ and the two modes $B_s^0 \rightarrow J/\psi\eta$ and $B_s^0 \rightarrow J/\psi\eta'$ [30, 31]. These measurements were interpreted as evidence for a sizeable glueball component in the η' meson, based on comparison with theoretical predictions for the branching fractions [27]. Results for the two B_s^0 modes were first reported by the LHCb collaboration using proton-proton (pp) collision data corresponding to an integrated luminosity of 1 fb^{-1} [32]. A second LHCb analysis, based on a larger integrated luminosity of 3 fb^{-1} , measured the four decay modes and found no evidence for a glueball component. The study determined the mixing angles to be $\phi_P = (43.5^{+1.4}_{-2.8})^\circ$ and $\phi_G = (0.0 \pm 24.6)^\circ$ [10].

This analysis uses the pp sample recorded by LHCb at centre-of-mass energies of 7, 8 and 13 TeV, corresponding to an integrated luminosity of 9 fb^{-1} , to determine the branching fraction ratios between $B_{(s)}^0 \rightarrow J/\psi\eta'$ and $B_{(s)}^0 \rightarrow J/\psi\eta$ decays, and subsequently the mixing angles. Ratios of branching fractions between the two B flavours for a given final state are also determined (Eqs. 7 and 8), although they are sensitive to ϕ_P only. The observables are measured as

$$R_{d,s} = \frac{N(B_{(s)}^0 \rightarrow J/\psi\eta')}{N(B_{(s)}^0 \rightarrow J/\psi\eta)} \cdot \frac{\varepsilon(B_{(s)}^0 \rightarrow J/\psi\eta)}{\varepsilon(B_{(s)}^0 \rightarrow J/\psi\eta')} \cdot \frac{\mathcal{B}(\eta \rightarrow f_\eta)}{\mathcal{B}(\eta' \rightarrow f_{\eta'})} \cdot \frac{\Phi^3(B_{(s)}^0 \rightarrow J/\psi\eta)}{\Phi^3(B_{(s)}^0 \rightarrow J/\psi\eta')}, \quad (9)$$

where the secondary branching fractions \mathcal{B} for the $\eta^{(\prime)}$ decays to the final states $f_{\eta^{(\prime)}}$ are used, and

$$R_{\eta^{(\prime)}} = \frac{N(B_s^0 \rightarrow J/\psi\eta^{(\prime)})}{N(B_s^0 \rightarrow J/\psi\eta^{(\prime)})} \cdot \frac{\varepsilon(B_s^0 \rightarrow J/\psi\eta^{(\prime)})}{\varepsilon(B^0 \rightarrow J/\psi\eta^{(\prime)})} \cdot \frac{f_s}{f_d} \cdot \frac{\Phi^3(B_s^0 \rightarrow J/\psi\eta^{(\prime)})}{\Phi^3(B^0 \rightarrow J/\psi\eta^{(\prime)})}, \quad (10)$$

where f_s/f_d is the ratio of b -quark fragmentation fractions governing the relative production of $B_{(s)}^0$ mesons.

Absolute branching fractions are calculated using the decay $B_s^0 \rightarrow J/\psi\phi$ as a normalisation channel. As suggested in Ref. [23], a complementary determination of the angle ϕ_P is possible using the measurement of $\mathcal{B}(B^0 \rightarrow J/\psi\eta)$ and the ratio

$$R_0 \equiv \frac{\mathcal{B}(B^0 \rightarrow J/\psi\eta)}{\mathcal{B}(B^0 \rightarrow J/\psi\pi^0)} \cdot \frac{\Phi^3(B^0 \rightarrow J/\psi\pi^0)}{\Phi^3(B^0 \rightarrow J/\psi\eta)} = \cos^2 \phi_P. \quad (11)$$

This determination uses the known branching fractions of $B^0 \rightarrow J/\psi\pi^0$ and $B_s^0 \rightarrow J/\psi\phi$ decays (the latter being used to determine $\mathcal{B}(B^0 \rightarrow J/\psi\eta)$) and is therefore less precise than that based on the $R_{d,s}$ ratios. It is nevertheless interesting as the ratio R_0 is sensitive to a possible glueball component in the η meson which would modify Eq. 11 as $R_0 = \cos^2 \phi_P \cdot \cos^2 \phi_G^\eta$, where ϕ_G^η is the corresponding mixing angle.

This analysis further improves upon the sensitivity of the previous LHCb analysis [10] by incorporating a second final state for the reconstruction of the $\eta^{(\prime)}$ mesons, allowing for two independent determinations of the branching fraction ratios, which are subsequently combined. The paper is organised as follows. A brief description of the experimental apparatus is given in Sec. 2 and the selection of signal and normalisation candidates are detailed in Sec. 3. The selection efficiencies are calculated using simulation in Sec. 4, while the yields of the various decays are determined from fits to the data, as explained in Sec. 5. Systematic uncertainties affecting the measurements of the branching fraction ratios and of the angles are presented in Sec. 6. Results for these observables are presented and briefly discussed in Sec. 7.

2 Detector description

The LHCb detector [33, 34] is a single-arm forward spectrometer covering the pseudorapidity range $2 < \eta < 5$, designed for the study of particles containing beauty or charm quarks. It includes a high-precision tracking system consisting of a silicon-strip vertex detector (VELO) surrounding the pp -interaction region, a large-area silicon-strip detector (TT) located upstream of a dipole magnet with a bending power of approximately

4 T m, and three stations of silicon-strip detectors and straw drift tubes placed downstream of the magnet. The tracking system provides a measurement of the momentum, p , of charged particles with a relative uncertainty that varies from 0.5 % at low momentum to 1.0 % at 200 GeV/ c . The minimum distance of a track to a primary vertex (PV), the impact parameter (IP), is measured with a resolution of $(15 + 29/p_T)$ μm , where p_T is the component of the momentum transverse to the beam, in GeV/ c . Various charged hadrons are distinguished using information from two ring-imaging Cherenkov detectors. In addition, photons, electrons, and hadrons are identified by a calorimeter system consisting of scintillating-pad and preshower detectors, an electromagnetic and a hadronic calorimeter. The electromagnetic calorimeter response is calibrated using samples of $\pi^0 \rightarrow \gamma\gamma$ decays [35]. Muons are identified by a system composed of alternating layers of iron and multiwire proportional chambers.

The online event selection is performed by a trigger, which consists of a hardware stage followed by a two-level software stage [36]. An alignment and calibration of the detector is performed in near real-time with the results used in the software trigger [37]. The same alignment and calibration information is propagated to the offline reconstruction, ensuring consistent information between the trigger and offline software. In this analysis, candidate events are required to pass the hardware trigger, which selects muon and dimuon candidates with high transverse momenta using information from the muon system. The first stage of the software trigger performs a partial event reconstruction and requires events to have two well-identified oppositely charged muons with an invariant mass larger than 2700 MeV/ c^2 . The second stage performs a full event reconstruction. Events are retained for further processing if they contain a displaced $J/\psi \rightarrow \mu^+\mu^-$ candidate. The decay vertex is required to be well separated from each reconstructed PV of the pp interaction by requiring the distance between the PV and the J/ψ decay vertex divided by its uncertainty to be greater than three.

Simulated pp collisions are generated using PYTHIA [38] with a specific LHCb configuration [39]. Decays of hadronic particles are described by EVTGEN [40], in which final-state radiation is generated using PHOTOS [41]. The interaction of the generated particles with the detector, and its response, are implemented using the GEANT4 toolkit [42] as described in Ref. [43]. The production of some samples is based on a computing-efficient model where the underlying pp interaction is reused multiple times, with an independently generated signal decay for each [44]. The resulting selection efficiencies are found to be compatible with those based on the default production model, with slightly larger uncertainties resulting from the residual correlation between reused events.

3 Selections

Signal candidates are reconstructed using $J/\psi \rightarrow \mu^+\mu^-$ decays, and the $\pi^+\pi^-\gamma$ (one-photon) and $\pi^+\pi^-\gamma\gamma$ (two-photon) final states of the $\eta^{(\prime)}$ decays, namely: $\eta \rightarrow \pi^+\pi^-\gamma$, $\eta' \rightarrow \rho^0(\rightarrow \pi^+\pi^-)\gamma$,² $\eta \rightarrow \pi^+\pi^-\pi^0(\rightarrow \gamma\gamma)$ and $\eta' \rightarrow \pi^+\pi^-\eta(\rightarrow \gamma\gamma)$. For the normalisation channel $B_s^0 \rightarrow J/\psi\phi$, the ϕ meson is reconstructed using the decay to $\pi^+\pi^-\pi^0$, with $\pi^0 \rightarrow \gamma\gamma$.

The two muons must satisfy $p_T > 500$ MeV/ c , pass a loose particle-identification (PID)

²Throughout the paper, the symbol ρ denotes the $\rho(770)$ resonance, and the presence of the ρ^0 resonance in the η' decay is omitted.

requirement and be unlikely to originate from a PV. Furthermore, their combination should form a good vertex that is significantly displaced from any PV, have a mass within $\pm 100 \text{ MeV}/c^2$ of the known J/ψ mass [45] and an IP value larger than $18 \mu\text{m}$. The J/ψ candidates are combined with pions and photons. The pions are required to have $p_T > 250 \text{ MeV}/c$ and be unlikely to originate from a PV. Similar to J/ψ candidates, a requirement is applied to the quality of the dipion vertex. In the $J/\psi\eta'(\rightarrow\pi^+\pi^-\gamma)$ final state only, the dipion mass is required to be larger than $500 \text{ MeV}/c^2$.

In the two-photon modes, photons must satisfy $p_T > 200 \text{ MeV}/c$ and be identified as well-isolated clusters in the electromagnetic calorimeter based on the response of a neural-net estimator trained to reject hadronic background. The diphoton combination must have $p_T > 500 \text{ MeV}/c$ ($1000 \text{ MeV}/c$) for $\eta \rightarrow \pi^+\pi^-\pi^0$ ($\eta' \rightarrow \pi^+\pi^-\eta$) decays, and a mass within $\pm 100 \text{ MeV}/c^2$ ($\pm 155 \text{ MeV}/c^2$) of the known π^0 (η) mass [45]. These mass windows are significantly broader than the experimental resolution, as required for the evaluation of systematic uncertainties later in the analysis. Diphoton and dipion candidates are then combined to form $\eta^{(\prime)}$ candidates, which are required to have $p_T > 2000 \text{ MeV}/c$. The mass of η (η') candidates must lie in the range $500\text{--}650 \text{ MeV}/c^2$ ($800\text{--}1200 \text{ MeV}/c^2$), which is also significantly broader than the experimental resolution.

In the one-photon modes, the photon p_T requirement is increased to $500 \text{ MeV}/c$ to reduce combinatorial background and the same requirement on cluster isolation is used. Moreover, a relatively wide mass window of $400\text{--}750 \text{ MeV}/c^2$ ($800\text{--}1200 \text{ MeV}/c^2$) is chosen for the η (η') candidates, which must also have $p_T > 2000 \text{ MeV}/c$.

The $\eta^{(\prime)}$ and J/ψ candidates are then combined and the four-track vertex is required to have good fit χ^2 and be significantly displaced from the PV that fits best to the flight direction of the $B_{(s)}^0$ candidate. Additionally, these candidates must have a mass in the range $4800\text{--}6200 \text{ MeV}/c^2$ and a p_T larger than $1800 \text{ MeV}/c$. To improve the $B_{(s)}^0$ mass resolution, a kinematic fit [46] is performed where each candidate is required to originate from the PV and the reconstructed masses of the intermediate narrow resonances (J/ψ , $\eta^{(\prime)}$, ϕ and π^0) are constrained to their known values. For the decay modes with two photons, a second kinematic fit is performed where the mass constraint on the $\pi^+\pi^-\gamma\gamma$ system is removed. This allows to improve the $\eta^{(\prime)}$ mass resolution and hence to reduce combinatorial background below the corresponding mass peaks, as described later in this section.

Further selections are based on a boosted decision tree (BDT) [47, 48] implemented in the TMVA toolkit [49]. This BDT classifier uses twelve variables which are accurately described by the simulation. These are related to the decay vertex, the kinematics of final-state particles, as well as the number of particles from the underlying event that are reconstructed close to the signal momentum direction, and their p_T . A total of eight classifiers are trained, one for each of the four signal final states and run periods (Run 1 from 2011 to 2012 and Run 2 from 2015 to 2018). The training samples consist of simulated B_s^0 decays and same-sign data candidates ($J/\psi\pi^+\pi^+\gamma(\gamma)$) for signal and background, respectively.

For a given final state, the BDT threshold and the size of the $\pi^+\pi^-\gamma(\gamma)$ and diphoton mass windows are chosen to maximise the significance of the B^0 signal defined as $S/\sqrt{S+B}$. Here, S and B are the expected B^0 yield and background contamination in the B^0 signal region, respectively, corresponding to approximately three times the B^0 mass resolution. They are determined using a fit to the $J/\psi\pi^+\pi^-\gamma(\gamma)$ mass distribution in data where the B^0 , B_s^0 and background yields are free to vary. Given the large uncertainty in the

B^0 yields, the value of S is inferred from the B_s^0 yield, the Run 1 value of ϕ_P , and other normalisation factors. At the chosen working points, the BDT selections reject 95–99% of background and retain 70–86% of the signal. The chosen mass windows correspond to $\pm 2\sigma$ in the two-photon modes, where σ represents the experimental resolution. In the one-photon modes, the η (η') mass window corresponds to $\pm 1\sigma$ ($\pm 1.5\sigma$).

Contamination from $B_{(s)}^0 \rightarrow J/\psi \pi^+ \pi^-$ decays can occur when the final-state particles are combined with a reconstructed photon in the event; and similarly for the decays $B^0 \rightarrow J/\psi K^+ \pi^-$, where, in addition, the kaon is misidentified as a pion. These backgrounds are only significant in the one-photon modes and are removed by rejecting signal candidates with a $J/\psi h^+ \pi^-$ mass, where h^+ is a kaon or a pion, in the vicinity of the known $B_{(s)}^0$ mass. The effect of these vetoes on the shape of the combinatorial background mass distribution is investigated using same-sign data and is found to be negligible.

The selection of normalisation $B_s^0 \rightarrow J/\psi \phi(\rightarrow \pi^+ \pi^- \pi^0)$ decays is largely aligned with that of $B_{(s)}^0 \rightarrow J/\psi \eta(\rightarrow \pi^+ \pi^- \pi^0)$ decays. Due to the larger phase space of the ϕ decay, the normalisation sample exhibits higher combinatorial background which is mitigated by a more stringent $\pi^0 p_T$ requirement of 1000 MeV/ c . Furthermore, dedicated BDT classifiers are trained using simulation where the ϕ meson decays to $\rho^+ \pi^-$, $\rho^- \pi^+$ or $\rho^0 \pi^0$. The BDT threshold and the ϕ and π^0 mass requirements are similar to those in the signal mode to minimise systematic uncertainties.

After all selections, about 1–2% of events contain multiple candidates, primarily due to the signal decays being reconstructed with an additional photon from the event. These candidates are not removed and are instead modelled in the fit, as detailed in Sec. 5.1.

4 Estimation of efficiencies

Selection efficiencies for the B_s^0 modes are calculated for each year of data taking using simulation, and then averaged according to the corresponding integrated luminosity and $b\bar{b}$ production cross-section. With a smaller set of simulated samples, the B^0 efficiency averages are calculated as the product of the B_s^0 averages and the B^0/B_s^0 efficiency ratios, where those ratios are obtained for the same data-taking conditions. The associated uncertainty is discussed in Sec. 6.

The $B_{(s)}^0$ efficiencies are corrected for small imperfections in the modelling of the $\eta^{(\prime)}$ lineshapes, in particular of their peak positions and widths. These corrections are derived from fits to the corresponding mass distributions in data, where only signal candidates in the vicinity of the B_s^0 peak are considered. Fits to the $\pi^+ \pi^- \gamma$, $\pi^+ \pi^- \pi^0$ and $\pi^+ \pi^- \eta$ mass distributions in data are shown in Fig. 1, where the signal and partially reconstructed background components are modelled using simulation (the signal peak position and width are free to vary in the data fits) and combinatorial background is modelled using same-sign data.

The lineshape corrections vary between 3 and 5% across the signal modes and partly cancel in the η/η' efficiency ratios, which are affected at the level of 1–3%. A second set of efficiency corrections addresses the modelling of diphoton lineshapes. In that case, samples of $B^+ \rightarrow J/\psi K^{*+}(\rightarrow K^+ \pi^0(\rightarrow \gamma\gamma))$ and $B_s^0 \rightarrow J/\psi \eta(\rightarrow \gamma\gamma)$ decays are used to constrain the diphoton lineshape parameters in signal data, which allows to determine the corrections with relatively small uncertainties.³ Diphoton corrections are at the level

³Throughout the paper, the $K^*(892)$ resonances are denoted as K^* .

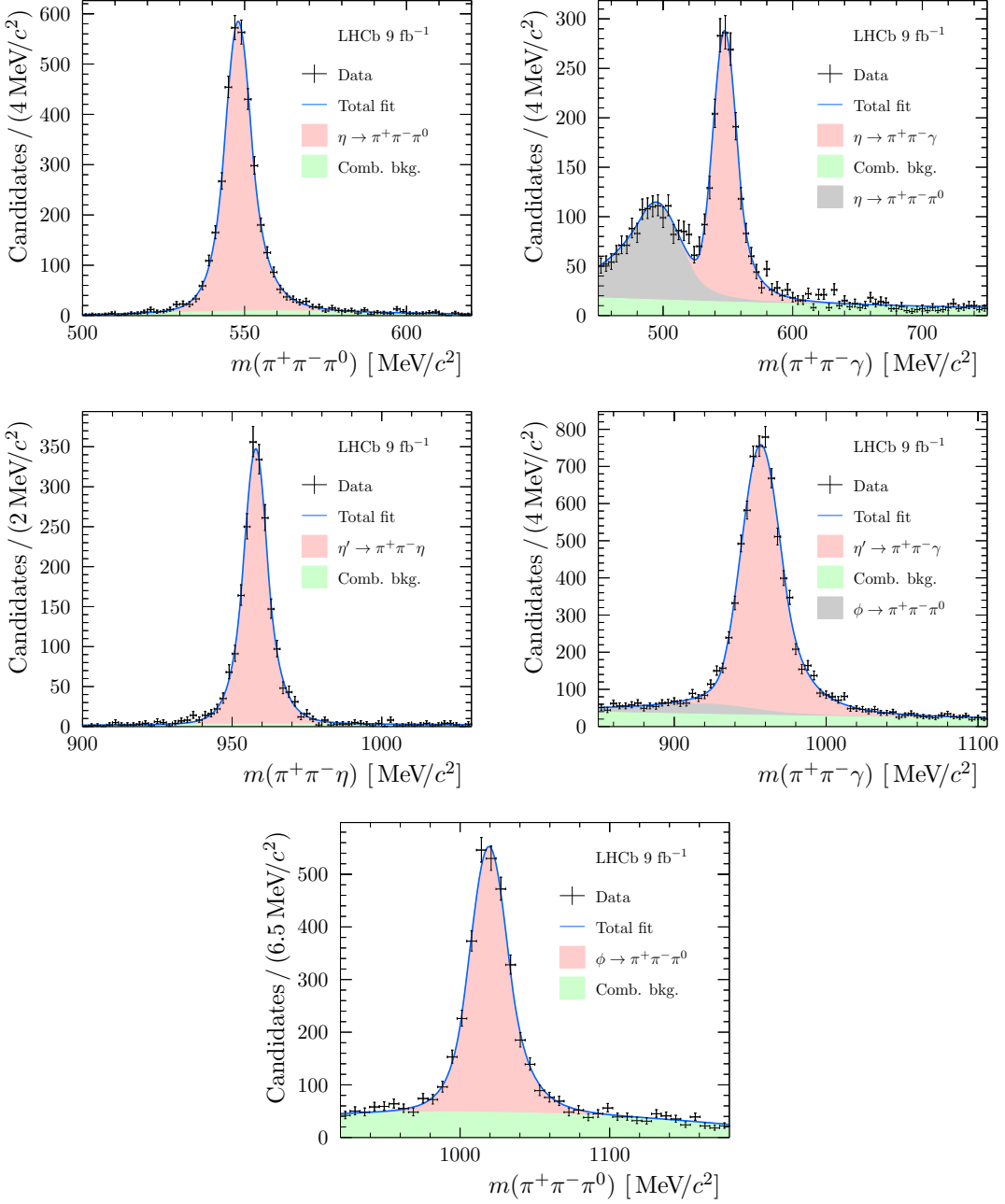


Figure 1: Mass distributions of (top) η , (middle) η' and (bottom) ϕ candidates in data. To enhance the purity, only $\eta^{(\prime)}$ (ϕ) candidates with a $J/\psi\eta^{(\prime)}$ ($J/\psi\phi$) mass close to the known B_s^0 mass are considered. The fit results show the stacked contributions from signal (in red), combinatorial background (in green) and partially reconstructed backgrounds (in gray).

of 2%, which drops to a negligible level when the η/η' efficiency ratios are considered.

Further efficiency corrections account for the small difference between the B_s^0 lifetime value used in the simulation, τ_{sim} , and the known value, τ , by assigning each simulated B_s^0 candidate the weight

$$w = \frac{\tau_{\text{sim}}}{\tau} \exp\left(-t\left(\frac{1}{\tau} - \frac{1}{\tau_{\text{sim}}}\right)\right), \quad (12)$$

where t is the true B_s^0 decay time. Given the small CP violation in the B_s^0 system and the CP -even nature of the signal final states, the approximation $\tau \approx \tau_L$ is used, where $\tau_L = 1.429 \pm 0.006$ ps corresponds to the known lifetime of the approximately CP -even (light) B_s^0 mass eigenstate [45]. On the other hand, both the light and heavy eigenstates decay to the $J/\psi\phi$ final state, in which case, the effective lifetime of 1.487 ps is used. This value is based on the mixing and amplitude parameters from Ref. [50] and enters the determination of the normalisation branching fraction, as detailed in Ref. [51]. Lifetime corrections amount to 8–9% and 2–3% in the signal and normalisation modes, respectively.

Additional corrections for the mismodelling of the pion PID response and $B_{(s)}^0$ kinematics largely cancel in the efficiency ratios and are therefore not applied. The associated uncertainties are discussed in Sec. 6.

5 Determination of the yields

5.1 Fit model

The $B_{(s)}^0$ yields are determined using unbinned extended maximum-likelihood fits to the $J/\psi\pi^+\pi^-\gamma(\gamma)$ mass distributions in the range 5150–5650 MeV/ c^2 . In the signal modes, the fit models account for the contributions from B^0 and B_s^0 decays and combinatorial background, whose yields are free to vary. Also, signal decays where one photon is replaced by another photon from the event, later referred to as random photon backgrounds, are modelled in the fits. Their yields are constrained to those of the signal decays based on ratios obtained from simulation. A similar model is used for the normalisation channel, except for the presence of the B^0 component which is expected to be negligible [52].

Signal contributions are modelled using a Gaussian function with a power-law tail on each side of the peak. All B_s^0 shape parameters are fixed from simulation, except the width which is scaled by a free parameter to account for the different resolution in data and simulation. Given the smaller size of the available B^0 simulated samples, the corresponding peak value μ_d and width σ_d parameters are expressed as a function of those of the B_s^0 modes as $\mu_d = \mu_s - \Delta_\mu$ and $\sigma_d = \sigma_s/R_\sigma$, where Δ_μ and R_σ are extracted from a simultaneous fit to the simulated B^0 and B_s^0 mass distributions. The B_s^0 tail parameters are also used for the B^0 shapes.

Random photon components are modelled by a modified Gaussian function with exponential tails. For each model, the B_s^0 parameters are determined using simulation and the signal scale factor is applied to the width. Also in this case, the B^0 mean and width parameters depend on those of the B_s^0 modes through Δ_μ and R_σ , while B_s^0 tail parameters are used for the B^0 shapes. The choice of parametrisation for the combinatorial background is motivated by the mass distribution in same-sign data. Except for the fit to the $J/\psi\eta'(\rightarrow\pi^+\pi^-\gamma)$ mass distribution whose model is further described in Sec. 5.1.2, an exponential function is used with a slope parameter that is free to vary. Partially reconstructed backgrounds from $B^{(0,+)} \rightarrow J/\psi\eta^{(\prime)}\pi^{(0,+)}$ decays, where the $\eta^{(\prime)}\pi$ system originates mainly from the $a_0(980)$ scalar resonance and the pion is not reconstructed, are expected to be quite small [53–55]. Moreover, this background should contribute outside the fit region and is thus ignored. Based on the branching fraction estimates from Ref. [56], similar contributions from B_s^0 decays are expected to be even smaller and are also neglected.

5.1.1 Backgrounds in the $J/\psi\eta(\rightarrow\pi^+\pi^-\gamma)$ sample

When one photon is missed, $B_s^0 \rightarrow J/\psi\eta(\rightarrow\pi^+\pi^-\pi^0)$ and $B_s^0 \rightarrow J/\psi\eta'(\rightarrow\pi^+\pi^-\eta)$ decays can satisfy the $J/\psi\eta(\rightarrow\pi^+\pi^-\gamma)$ selection criteria. Their contributions relative to the B_s^0 signal are estimated to be 12% and 7%, respectively, based on the known $\eta^{(\prime)}$ branching fractions [45] and simulated selection efficiencies. The estimation of the second background contribution also requires knowledge of the branching fraction ratio between $B_s^0 \rightarrow J/\psi\eta$ and $B_s^0 \rightarrow J/\psi\eta'$ decays, which is calculated using the ϕ_P and ϕ_G values from the Run 1 analysis. The relative fractions of these two background contributions in the $J/\psi\eta(\rightarrow\pi^+\pi^-\gamma)$ fit are then fixed. Their shapes are modelled by a modified Gaussian function with exponential tails whose parameters are constrained using simulation. Also in this case, the signal scale factor is applied to the width of the modified Gaussian functions. Given their smaller branching fractions, the corresponding backgrounds from B^0 decays are neglected. The potential background contribution from $B^0 \rightarrow J/\psi\omega(\rightarrow\pi^+\pi^-\pi^0)$ decays with one π^0 photon not reconstructed is studied and found to be negligible.

5.1.2 Backgrounds in the $J/\psi\eta'(\rightarrow\pi^+\pi^-\gamma)$ sample

Due to the larger dipion mass allowed in $B_{(s)}^0 \rightarrow J/\psi\eta'(\rightarrow\pi^+\pi^-\gamma)$ decays, this sample includes additional background sources, such as $B_s^0 \rightarrow J/\psi\phi(\rightarrow\pi^+\pi^-\pi^0)$ decays in which one photon from the π^0 decay is not reconstructed. To reduce the correlation between the yield of that background and that of combinatorial background, the former is fixed to the value measured in the normalisation sample scaled by the ratio of efficiencies in simulation for the partial and full reconstruction of the decay. Its shape is modelled by the product of an increasing and a decreasing sigmoid function, whose inflection points and widths are determined from simulation. Furthermore, contributions from $B^{(0,+)} \rightarrow J/\psi K^{(0,+)}\pi^+\pi^-$ decays with a kaon not reconstructed and an additional photon from the event are modelled using a modified Gaussian function with a power-law tail on the right side of the peak. The shape is determined from simulated $B^+ \rightarrow J/\psi K_1(1270)^+$ decays where both the $K^{*0}\pi^+$ and $K^+\rho^0$ intermediate states of the $K_1(1270)^+$ meson are considered, as well as direct $K_1(1270)^+ \rightarrow K^+\pi^+\pi^-$ decays. The corresponding yield is left free to vary in the fit. Finally, the combinatorial background is modelled by the product of a Gaussian and an exponential function, which accounts for the depletion of candidates at lower masses. Given the presence of the aforementioned peaking backgrounds in that region, the shape parameters are fixed using a fit to same-sign data while the yield is free to vary.

5.2 Fit results

The mass distributions for the signal and normalisation modes are shown in Fig. 2, with fit results included. The yields of $B_{(s)}^0$ decays in the signal and normalisation samples are listed in Table 1. For the signal modes, a 1–5% correlation between the B^0 and B_s^0 yields is observed, which is slightly more pronounced in the one-photon modes. The B^0/B_s^0 yield ratios are also shown to emphasise the agreement between one-photon and two-photon results. Statistical uncertainties at the level of 1–3% and 8–17% are obtained for the B_s^0 and B^0 modes, respectively.

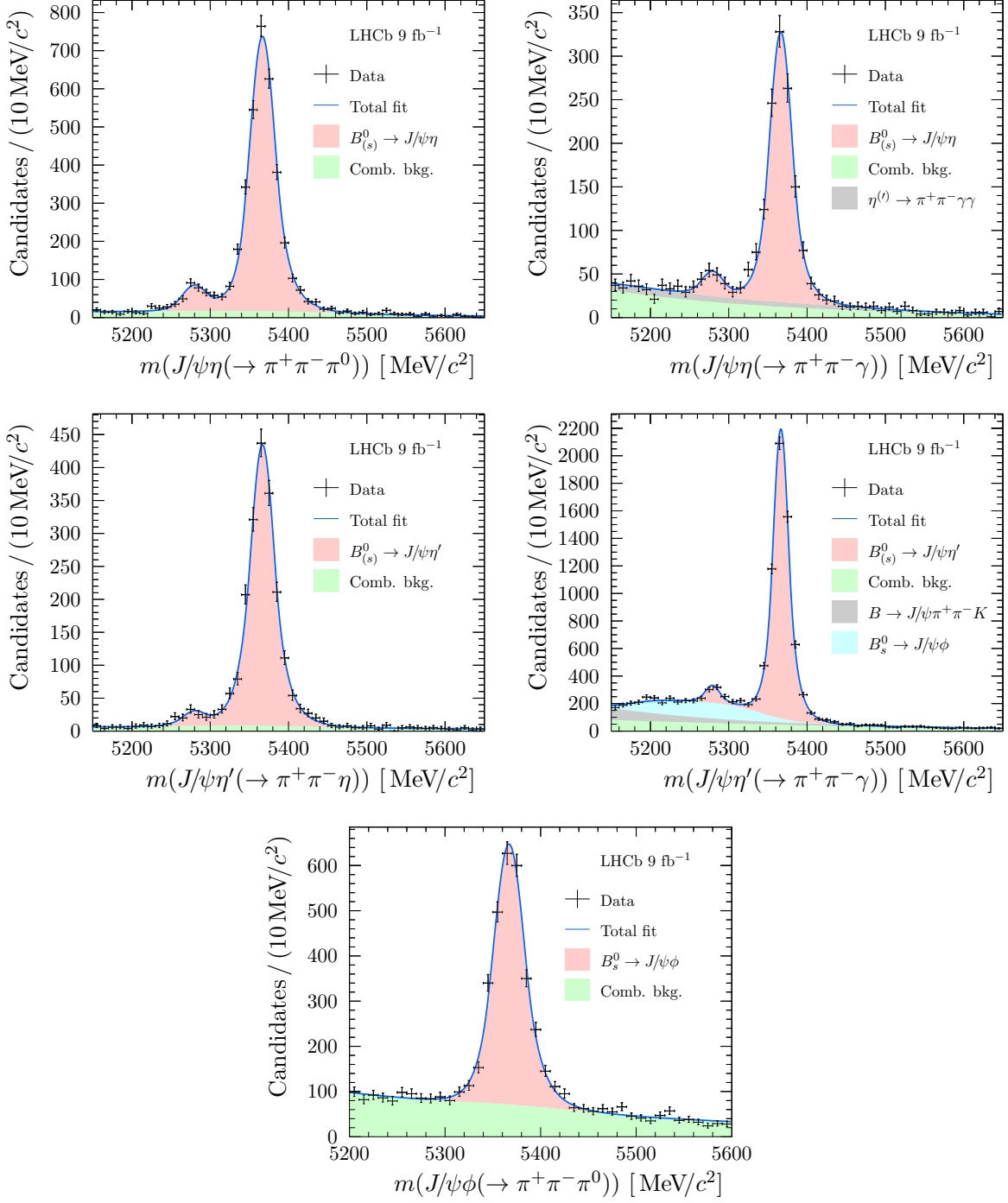


Figure 2: Mass distributions of $B_{(s)}^0$ candidates in data reconstructed in the (top) $J/\psi\eta$, (middle) $J/\psi\eta'$ and (bottom) $J/\psi\phi$ final states. The fit results show the stacked contributions from signal (in red), combinatorial and random-photon backgrounds (in green) and partially reconstructed backgrounds (in gray or light blue).

6 Systematic uncertainties

The main sources of systematic uncertainties on the branching fraction ratios are summarised in Table 2. They pertain to the determination of the $B_{(s)}^0$ yields (Sec. 6.1), the

Table 1: Yields $N_{d,s}$ of $B_{(s)}^0$ decays in the signal and normalisation channels for different final states. The ratio and correlation coefficient (ρ_{ds}) between the signal yields are also indicated.

	Decay mode				
	$B_{(s)}^0 \rightarrow J/\psi\eta$		$B_{(s)}^0 \rightarrow J/\psi\eta'$		$B_s^0 \rightarrow J/\psi\phi$
	$\eta \rightarrow \pi^+\pi^-\pi^0$	$\eta \rightarrow \pi^+\pi^-\gamma$	$\eta' \rightarrow \pi^+\pi^-\eta$	$\eta' \rightarrow \pi^+\pi^-\gamma$	$\phi \rightarrow \pi^+\pi^-\pi^0$
N_d	285 ± 23	110 ± 18	94 ± 14	355 ± 38	–
N_s	3280 ± 60	1244 ± 40	1885 ± 45	6002 ± 85	2572 ± 62
$N_d/N_s [10^{-2}]$	8.7 ± 0.7	8.9 ± 1.5	5.0 ± 0.8	5.9 ± 0.7	–
$\rho_{ds} [10^{-2}]$	–2.3	–5.1	–1.5	4.6	–

Table 2: Summary of relative uncertainties affecting the branching fraction ratios, in percent. In the two last columns, $R_{\eta(\eta'),\phi}^{\gamma\gamma}$ are the ratios between B_s^0 signal and normalisation modes, determined using the final states with two photons.

Source	$R_d^{\gamma\gamma}$	R_d^γ	$R_s^{\gamma\gamma}$	R_s^γ	$R_\eta^{\gamma\gamma}$	R_η^γ	$R_{\eta'}^{\gamma\gamma}$	$R_{\eta'}^\gamma$	$R_{\eta,\phi}^{\gamma\gamma}$	$R_{\eta',\phi}^{\gamma\gamma}$
Fit model	4.2	7.8	0.5	2.4	1.0	4.9	4.1	6.5	1.9	1.9
Lineshape	1.7	2.4	1.7	2.4	–	–	–	–	1.2	1.6
Photon p_T	1.7	0.4	1.7	0.4	–	–	–	–	0.2	1.5
BDT response	2.7	1.5	2.7	1.5	–	–	–	–	0.5	2.6
Sim. sample size	2.8	3.2	1.8	1.7	1.8	3.0	2.9	2.2	1.5	1.8
Decay model	–	–	–	–	–	–	–	–	2.2	2.2
Total syst. unc.	6.2	8.9	4.1	4.1	2.1	5.8	5.1	6.9	3.6	4.9
External inputs	1.7	2.1	1.7	2.1	3.1	3.1	3.1	3.1	2.9	3.0
Stat. unc.	17.0	19.6	3.0	3.5	8.2	16.8	15.2	10.6	3.1	3.4

evaluation of the efficiencies and their associated corrections (Sec. 6.2), and the precision of the various inputs that enter the calculation of the ratios (Sec. 6.3).

6.1 Fit model uncertainties

The systematic uncertainties affecting the signal yields through the choice of fit models are determined by changing the shape of all components and repeating the fits. For the components that are fixed relative to the signal, the corresponding fraction is also changed. The different sources are grouped as follows.

Except for the combinatorial background, all the baseline parametrisations are determined using simulation. Either these are changed to nonparametric functions, which, in the case of the signal shapes, are convolved with a Gaussian function to account for resolution effects, or new parameters are randomly generated using the baseline models and covariance matrices.

The difference between the B^0 and B_s^0 lineshapes, encoded in the Δ_μ and R_σ parameters, is accounted for by varying these parameters according to their baseline values and uncertainties. Similarly, the normalisation of the random photon components relative

to the signal are varied according to the uncertainties of the corresponding simulation efficiencies. For the peaking backgrounds that are constrained relative to the signal, the normalisation is changed according to the uncertainties of the simulated efficiency and known branching fractions.

In the normalisation mode, the B_s^0 peak is described based on simulated resonant ϕ decays. Given that the Dalitz plot in data does not reveal resonant structures, a smaller sample of nonresonant $\phi \rightarrow \pi^+ \pi^- \pi^0$ decays is used as an alternative model, from which a systematic uncertainty is derived. In the case of the $J/\psi\eta'(\rightarrow \pi^+ \pi^- \gamma)$ model, the fixed $B_s^0 \rightarrow J/\psi\phi(\pi^+ \pi^- \pi^0)$ background yield is varied according to the uncertainties of the yield measured in full reconstruction. The influence of the ϕ decay model on the efficiency is also accounted for.

For the final states other than $J/\psi\eta'(\rightarrow \pi^+ \pi^- \gamma)$, the exponential slope parameter describing the combinatorial background is randomly drawn from a Gaussian distribution. The Gaussian mean and width are set to the value and uncertainty of the slope parameter as obtained from a fit to same-sign data in a wide mass region of 4800–6200 MeV/ c^2 . For the $J/\psi\eta'(\rightarrow \pi^+ \pi^- \gamma)$ final state, the baseline model is changed to an exponential function and the same procedure is applied. However, the fit to same-sign data is now performed in the baseline fit region of 5150–6150 MeV/ c^2 to avoid the low-mass region where the distribution flattens.

In summary, model uncertainties mainly impact the B^0 yields through their sensitivity to the choice of background parametrisations, with values in the range 1–7% for the different final states. Uncertainties for the B_s^0 yields are negligibly small in the two-photon modes and reach 1–2% in the one-photon modes, reflecting the larger background contributions. These are propagated to the branching fraction ratios, with values between 0.5–7.8%, depending on which modes are combined.

6.2 Selection efficiency uncertainties

Efficiencies are calculated using simulation, under the assumption that small discrepancies between simulation and data in the modelling of selection variables cancel in the studied ratios. The corresponding uncertainties are estimated either by correcting the simulation, as done for the $\eta^{(\prime)}$ lineshapes and B_s^0 lifetime, or by using control modes, as done for the BDT response.

Corrections to the efficiency of the $\eta^{(\prime)}$ mass requirements are determined from fits to the corresponding lineshapes in data (Fig. 1). The statistical uncertainties on the fit parameters are propagated to the correction factors by generating several alternative normalised $\eta^{(\prime)}$ shapes, and calculating the efficiency as the integral of these functions in the relevant mass intervals. The relative variations of the efficiency range from 1–2% for each decay mode, which are added quadratically when considering the η'/η efficiency ratios, resulting in systematic uncertainties of 1.7% and 2.4% in the two-photon and one-photon modes, respectively. Uncertainties for the diphoton mass requirements contribute to an uncertainty at the subpercent level, where the same method is used, together with additional lineshape constraints from $B_s^0 \rightarrow J/\psi\eta(\rightarrow \gamma\gamma)$ and $B^+ \rightarrow J/\psi K^{*+}(\rightarrow K^+\pi^0(\rightarrow \gamma\gamma))$ samples. This study is performed for the normalisation channel, where uncertainties on the $\phi/\eta^{(\prime)}$ efficiency ratios between 1.2% and 1.6% are found.

Mismodelling of the BDT classifier inputs is studied in two parts. First, the photon p_T distributions in data and simulation are compared using the $B^+ \rightarrow J/\psi K^{*+}$ samples.

For each year of data taking, weights are determined in bins of photon p_T as the ratio of the normalised distributions, and applied to simulated signal candidates. To account for the statistical uncertainty of the B^+ signal, the assigned weights are randomly drawn from a Gaussian distribution with the mean and width set to the per-bin value and uncertainty of the weights. The influence of the photon p_T modelling is then estimated by calculating the signal BDT efficiencies using the sum of weights instead of the number of selected candidates. The change in the η/η' efficiency ratio is equal to 1.7% and 0.4% in the two-photon and one-photon modes, respectively, which are assigned as systematic uncertainties. This study is performed for the normalisation channel, yielding 0.2% and 1.5% for the η/ϕ and η'/ϕ efficiency ratio, respectively.

Control samples are used to assign the uncertainty for the modelling of the other classifier inputs. The decay $B^0 \rightarrow J/\psi \rho^0 (\rightarrow \pi^+ \pi^-)$ is used as a proxy to the signal mode $B_{(s)}^0 \rightarrow J/\psi \eta' (\rightarrow \pi^+ \pi^- \gamma)$. For the other three signal modes, which have a lower dipion mass, the decay $B^+ \rightarrow \psi(2S) (\rightarrow J/\psi \pi^+ \pi^-) K^+$ is used instead. New classifiers are trained without photon p_T information, using the baseline signal and background samples, and are then applied to the control mode candidates. The BDT efficiencies in data are then determined by fits to the B^0 or B^+ mass distributions in data, for candidates passing or failing the requirements. The efficiency ratios between data and simulation depart from unity by -7% to -3% , depending on the control mode and BDT requirement considered. These variations partly cancel in the double ratios, for which values of 2.7% and -1.5% are obtained in the two-photon and one-photon modes, respectively, and assigned as systematic uncertainties. In the normalisation channel, the uncertainties are 0.5% and 2.6% for the η/ϕ and η'/ϕ efficiency ratio, respectively.

The uncertainties related to the finite size of the simulated samples range from 0.7–1.6% in the B_s^0 signal mode to 1.5–2.6% in the B^0 modes for which fewer samples are available. In the normalisation mode, this uncertainty contributes to 1.1%, with an additional 2.2% contribution from the limited number of nonresonant ϕ decays used for an alternative efficiency determination.

Other subleading uncertainties arise from the lifetime corrections, and the modelling of the $B_{(s)}^0$ kinematics and pion PID. The uncertainties associated to the B_s^0 lifetime corrections in simulation are below the percent level, as verified by varying the known values of τ_L or the effective lifetime from Ref. [51], and are thus neglected. The modelling of the $B_{(s)}^0$ kinematics is judged based on the comparison of p_T and pseudorapidity distributions of $B^0 \rightarrow J/\psi K^{*0} (\rightarrow K^+ \pi^-)$ and $B_s^0 \rightarrow J/\psi \phi (\rightarrow K^+ K^-)$ decays in data and simulation, and is also found to have a negligible effect on the results. Similarly, the calibration of the pion PID response would change the efficiency ratios by half a percent. As a result, no correction is applied and the corresponding uncertainties are ignored.

In summary, the dominant sources of systematic uncertainties on the $R_{d,s}$ ratios in the evaluation of efficiencies arise from mismodelling of the $\eta^{(\prime)}$ lineshapes and the BDT response, and the finite size of the simulated samples. For the $R_{\eta^{(\prime)}}$ ratios, only the latter source is relevant.

6.3 External input uncertainties

The physical quantities used to determine the $R_{d,s}$ ratios are the branching fractions of the reconstructed $\eta^{(\prime)}$, ϕ and π^0 decays [45], and the phase-space factors defined in Eq. 4. The latter are a function of the masses of the $B_{(s)}^0$, J/ψ and $\eta^{(\prime)}$ mesons [45], whose

uncertainties are small enough to be ignored. The extraction of the angle ϕ_P from the $R_{\eta^{(\prime)}}$ ratios relies on the knowledge of the $B_{(s)}^0$ masses and lifetimes, the ratio of CKM elements $|V_{cd}/V_{cs}|^2$, and the hadronisation fraction f_s/f_d , which is also relevant for the determination of the absolute branching fractions. The hadronisation of b quarks to a $B_{(s)}^0$ meson is known to depend on its transverse momentum and on the pp centre-of-mass energy, as measured in Ref. [51], which reported f_s/f_d values for an average p_T of 5 GeV/ c of the decaying B mesons used in that measurement. Due to the higher reconstruction thresholds for decays with photons, the average B -meson p_T in the signal modes is larger, about 10 GeV/ c , resulting in slightly different f_s/f_d values. Updated values are determined using the p_T -parametrisations proposed in Ref. [51] by assigning a per-event f_s/f_d value to simulated signal candidates, keeping the relative uncertainties from the published values. At $\sqrt{s} = 13$ TeV for instance, the obtained averages are 3.7% smaller than the published values. All the aforementioned physical quantities are listed in Table 3.

Table 3: External inputs used in the determination of the branching fraction observables.

Physical quantity	Value	Reference
$\mathcal{B}(\eta \rightarrow \gamma\gamma)$	$(39.36 \pm 0.18)\%$	[45]
$\mathcal{B}(\eta \rightarrow \pi^+\pi^-\pi^0)$	$(23.02 \pm 0.25)\%$	
$\mathcal{B}(\eta \rightarrow \pi^+\pi^-\gamma)$	$(4.28 \pm 0.07)\%$	
$\mathcal{B}(\eta' \rightarrow \gamma\gamma)$	$(2.307 \pm 0.033)\%$	
$\mathcal{B}(\eta' \rightarrow \pi^+\pi^-\eta)$	$(42.5 \pm 0.5)\%$	
$\mathcal{B}(\eta' \rightarrow \pi^+\pi^-\gamma)$	$(29.5 \pm 0.4)\%$	
$\mathcal{B}(\pi^0 \rightarrow \gamma\gamma)$	$(98.823 \pm 0.034)\%$	
$\mathcal{B}(\phi \rightarrow \pi^+\pi^-\pi^0)$	$(15.4 \pm 0.4)\%$	
$m(B_s^0)$ [MeV/ c^2]	5366.93 ± 0.10	
$m(B^0)$ [MeV/ c^2]	5279.72 ± 0.08	
$m(J/\psi)$ [MeV/ c^2]	3096.900 ± 0.006	[45]
$m(\eta)$ [MeV/ c^2]	547.862 ± 0.017	
$m(\eta')$ [MeV/ c^2]	957.78 ± 0.06	
$\Phi^3(B^0 \rightarrow J/\psi\eta) / \Phi^3(B_s^0 \rightarrow J/\psi\eta)$	0.9436	
$\Phi^3(B^0 \rightarrow J/\psi\eta') / \Phi^3(B_s^0 \rightarrow J/\psi\eta')$	0.9255	
$\Phi^3(B^0 \rightarrow J/\psi\eta) / \Phi^3(B^0 \rightarrow J/\psi\eta')$	1.2668	
$\Phi^3(B_s^0 \rightarrow J/\psi\eta) / \Phi^3(B_s^0 \rightarrow J/\psi\eta')$	1.2424	
τ_L [s $^{-1}$]	$(1.429 \pm 0.006) \times 10^{-12}$	[45]
τ_{eff} [s $^{-1}$]	1.487×10^{-12}	[51]
f_s/f_d (7 TeV)	0.2390 ± 0.0076	
f_s/f_d (8 TeV)	0.2385 ± 0.0075	
f_s/f_d (13 TeV)	0.2539 ± 0.0079	[51]
f_s/f_d (Run 1+2)	0.2504 ± 0.0078	
V_{cd}	$0.22487^{+0.00024}_{-0.00021}$	
V_{cs}	$0.973521^{+0.000057}_{-0.000062}$	[57]

7 Results

7.1 Relative branching fractions

The obtained branching fraction ratios for signal decays of a given B flavour to $J/\psi\eta$ and $J/\psi\eta'$ mesons determined in the two-photon final states, $R_{d,s}^{\gamma\gamma}$, and in the one-photon final states, $R_{d,s}^\gamma$, are

$$\begin{aligned} R_d^{\gamma\gamma} &= 0.58 \pm 0.10 \pm 0.04 \pm 0.01, \\ R_d^\gamma &= 0.67 \pm 0.13 \pm 0.06 \pm 0.01, \\ R_s^{\gamma\gamma} &= 1.01 \pm 0.03 \pm 0.04 \pm 0.02, \\ R_s^\gamma &= 0.97 \pm 0.03 \pm 0.03 \pm 0.02, \end{aligned}$$

where the first uncertainties are statistical, the second are systematic, and the third relates to the precision of the $\eta^{(\prime)}$ branching fractions. The determinations of R_d or R_s obtained using the two different final states are compatible within one standard deviation.

Possible biases in the central values of $R_{d,s}$ and the accuracy of their statistical uncertainty estimates are assessed by means of pseudoexperiments. Using the baseline mass fit results, 10^4 pseudoexperiments are generated for each final state and the corresponding mass distributions are fitted with the baseline models. The obtained sets of yields are then combined to calculate the distributions of the $R_{d,s}^{\gamma(\gamma)}$ ratios. For most of the ratios, the biases in the central values are below 3% of the statistical uncertainties, and the Gaussian widths of the distributions depart from one by less than 1%, so no corrections are applied. For the R_d^γ ratio, a bias of 11% and slightly asymmetric uncertainties are found. In that case, the bias is ignored and symmetric uncertainties are assumed, taking the largest of the uncertainties on either sides of the R_d^γ distribution. Using the pseudoexperiments, the correlation between the R_d and R_s ratios is found to be small, below -1.6% and 5.3% in the two-photon and one-photon modes, respectively.

The branching fraction ratios between signal decays to a given $J/\psi\eta^{(\prime)}$ final state for different flavours of the B mesons are

$$\begin{aligned} R_\eta^{\gamma\gamma} &= (2.30 \pm 0.19 \pm 0.05 \pm 0.07) \times 10^{-2}, \\ R_\eta^\gamma &= (2.25 \pm 0.38 \pm 0.13 \pm 0.07) \times 10^{-2}, \\ R_{\eta'}^{\gamma\gamma} &= (1.31 \pm 0.20 \pm 0.07 \pm 0.04) \times 10^{-2}, \\ R_{\eta'}^\gamma &= (1.56 \pm 0.17 \pm 0.11 \pm 0.05) \times 10^{-2}, \end{aligned}$$

where the third uncertainties are associated to the precision of f_s/f_d . The determinations of R_η or $R_{\eta'}$ in the one-photon and two-photon modes are compatible within one standard deviation. Using the phase-space factors from Table 3, the following weighted average

ratios of branching fractions are obtained:

$$\begin{aligned}\frac{\mathcal{B}(B^0 \rightarrow J/\psi\eta')}{\mathcal{B}(B^0 \rightarrow J/\psi\eta)} &= 0.48 \pm 0.06 \pm 0.02 \pm 0.01, \\ \frac{\mathcal{B}(B_s^0 \rightarrow J/\psi\eta')}{\mathcal{B}(B_s^0 \rightarrow J/\psi\eta)} &= 0.80 \pm 0.02 \pm 0.02 \pm 0.01, \\ \frac{\mathcal{B}(B^0 \rightarrow J/\psi\eta)}{\mathcal{B}(B_s^0 \rightarrow J/\psi\eta)} &= (2.16 \pm 0.16 \pm 0.05 \pm 0.07) \times 10^{-2}, \\ \frac{\mathcal{B}(B^0 \rightarrow J/\psi\eta')}{\mathcal{B}(B_s^0 \rightarrow J/\psi\eta')} &= (1.33 \pm 0.12 \pm 0.05 \pm 0.04) \times 10^{-2},\end{aligned}$$

which are compatible with previous determinations [10] and are more precise. The ratios of branching fractions between signal and normalisation are measured in the two-photon modes only, yielding

$$\begin{aligned}\frac{\mathcal{B}(B_s^0 \rightarrow J/\psi\eta)}{\mathcal{B}(B_s^0 \rightarrow J/\psi\phi)} &= (4.50 \pm 0.14 \pm 0.16 \pm 0.13) \times 10^{-1}, \\ \frac{\mathcal{B}(B_s^0 \rightarrow J/\psi\eta')}{\mathcal{B}(B_s^0 \rightarrow J/\psi\phi)} &= (3.70 \pm 0.13 \pm 0.18 \pm 0.11) \times 10^{-1},\end{aligned}$$

where the last uncertainties reflect the precision of the $\eta^{(\prime)}$ and ϕ branching fractions.

7.2 Absolute branching fractions

The branching fractions of the signal B_s^0 modes are calculated using the $\eta^{(\prime)}/\phi$ ratios from Sec. 7.1 and the known value of the normalisation branching fraction, $\mathcal{B}(B_s^0 \rightarrow J/\psi\phi)$, given by $(1.018 \pm 0.032 \pm 0.037) \times 10^{-3}$ [51], with the first uncertainty including a contribution from f_s/f_d . The results are

$$\begin{aligned}\mathcal{B}(B_s^0 \rightarrow J/\psi\eta) &= (4.58 \pm 0.14 \pm 0.16 \pm 0.26) \times 10^{-4}, \\ \mathcal{B}(B_s^0 \rightarrow J/\psi\eta') &= (3.76 \pm 0.13 \pm 0.19 \pm 0.21) \times 10^{-4},\end{aligned}$$

where the last uncertainties reflect the precision of the normalisation branching fraction. The results for the B^0 decays, obtained by multiplying the B_s^0 branching fractions by the B^0/B_s^0 ratios reported in Sec. 7.1, are

$$\begin{aligned}\mathcal{B}(B^0 \rightarrow J/\psi\eta) &= (9.92 \pm 0.79 \pm 0.42 \pm 0.46) \times 10^{-6}, \\ \mathcal{B}(B^0 \rightarrow J/\psi\eta') &= (5.06 \pm 0.48 \pm 0.32 \pm 0.24) \times 10^{-6}.\end{aligned}$$

In these calculations, uncertainties from the two-photon B_s^0 modes are counted twice but remain marginal compared to those of the B^0 results. On the other hand, the contribution from f_s/f_d is removed.

The four results are compatible with the world averages [45] and more precise by a factor of 1.3–4.0, depending on the decay mode. The precision of the B^0 results is still limited by statistics, whereas systematic uncertainties and external inputs dominate the B_s^0 results.

7.3 Mixing angles

Given the correlation between the ϕ_P and ϕ_G values determined using Eqs. 2 and 3, the central values and uncertainties on these observables are calculated by constructing the two-dimensional likelihood function. Similar to the Run 1 analysis [10], this function is defined as

$$\mathcal{L} = \exp\left(-\frac{1}{2}\left[\left(\frac{\tan^2 \phi_P \cos^2 \phi_G - R_d}{\sigma_{R_d}^2}\right)^2 + \left(\frac{\cot^2 \phi_P \cos^2 \phi_G - R_s}{\sigma_{R_s}^2}\right)^2\right]\right), \quad (13)$$

where $R_{d,s}$ and $\sigma_{R_{d,s}}$ are the central values and total uncertainties of the ratios, respectively, as found using the one-photon or two-photon final states. A graphical representation of the two results and their combination is shown in Fig. 3, where regions corresponding to different confidence intervals are indicated. Numerical results for the central values and uncertainties of the angles are obtained by profiling the likelihood with respect to each of these two parameters separately for the one-photon and two-photon modes. For the combined results, the product of the two likelihood functions is used, which yields

$$\begin{aligned} \phi_P &= (41.6^{+1.0}_{-1.2})^\circ, \\ \phi_G &= (28.1^{+3.9}_{-4.0})^\circ. \end{aligned}$$

These two results are compatible with the Run 1 determination and supersede it. The measured η/η' mixing angle is compatible with values found in the literature. The gluonic angle ϕ_G departs from zero by more than four standard deviations, as evaluated using Wilks' theorem [58], representing the most precise measurement of this angle to date. Besides the increased data sample and the use of a second final state to reconstruct the $\eta^{(\prime)}$ mesons, the improvement in precision compared to the Run 1 result is also attributed to the fact that the uncertainty on ϕ_G depends on its measured value. This effect can be seen in Fig. 3 where the likelihood contours are stretched towards low ϕ_G values, as expected from the corresponding smaller impact of the glueball component on the $B_{(s)}^0 \rightarrow J/\psi \eta'$ decay rates.

It is interesting to note that Eqs. 7 and 8 lead to different determinations of ϕ_P , with values of $(46.9 \pm 0.6)^\circ$ and $(36.6 \pm 0.7)^\circ$, respectively. Because these equations rely on the cancellation of hadronic contributions to the amplitude of B^0 and B_s^0 decays to a given final-state, this discrepancy points to significant SU(3)-flavour breaking in these decays.

The angle ϕ_P is also determined through the ratio R_0 defined in Eq. 11. Using the branching fraction of $B^0 \rightarrow J/\psi \eta$ decays determined by this analysis and the known value for $B^0 \rightarrow J/\psi \pi^0$ decays [45], the obtained value is $R_0 = 0.66 \pm 0.08$, yielding $\phi_P = (35.7 \pm 4.7)^\circ$, which is compatible with the above $R_{d,s}$ -based determination. As explained in Sec. 1, a possible glueball component in the η meson would decrease the ratio R_0 , implying a smaller value of ϕ_P , and is therefore disfavoured.

8 Conclusions

An updated measurement of the $B_s^0 \rightarrow J/\psi \eta^{(\prime)}$ branching fractions is presented, based on a sample of pp collision data collected by the LHCb detector corresponding to an integrated luminosity of 9 fb^{-1} . A comparison of the branching fraction ratios to predictions from standard η/η' mixing, which requires only one mixing angle ϕ_P to describe the data, reveals

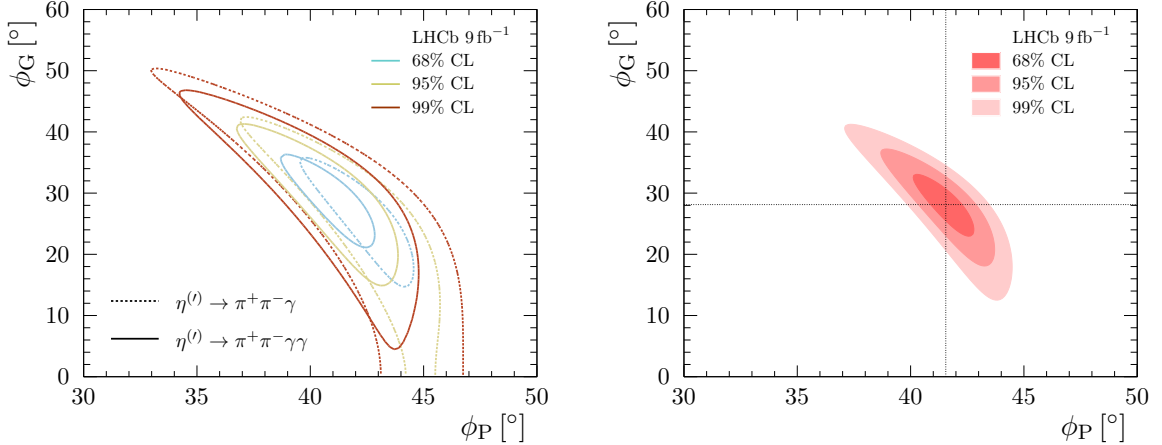


Figure 3: Contours of the two-dimensional likelihood function of ϕ_P and ϕ_G , corresponding to the one (68% confidence limit, CL), two (95% CL) and three (99% CL) sigma regions, for (left) the one-photon and two-photon modes, and (right) the combination of these two results. The dotted lines on the right plot indicate the central values.

a deficit of $B_{(s)}^0 \rightarrow J/\psi \eta'$ decays relative to the η modes. This result can be explained by a glueball component to the η' wave function and/or unexpectedly large contributions from gluon-mediated processes to the decay rates. Parametrising the glueball component by a second angle ϕ_G , a relatively large value of $(28.1^{+3.9}_{-4.0})^\circ$ is found, which differs from zero by more than four standard deviations. An $\eta/\eta^{(\prime)}$ mixing angle ϕ_P of $(41.6^{+1.0}_{-1.2})^\circ$ is determined, which is compatible and of similar precision to existing phenomenological determinations. Absolute branching fractions are also updated using the $B_s^0 \rightarrow J/\psi \phi$ channel as a normalisation. Significantly more precise values than the world averages are obtained, with factors ranging from 1.3–4.0 depending on the decay mode. The presented results supersede those of the Run 1 analysis based on 3 fb^{-1} of integrated luminosity. With the precision of the angle measurements being limited by the yields in the B^0 channels, significant improvements are expected in Run 3, based on the data from the upgraded LHCb detector.

Acknowledgements

We express our gratitude to our colleagues in the CERN accelerator departments for the excellent performance of the LHC. We thank the technical and administrative staff at the LHCb institutes. We acknowledge support from CERN and from the national agencies: ARC (Australia); CAPES, CNPq, FAPERJ and FINEP (Brazil); MOST and NSFC (China); CNRS/IN2P3 (France); BMBF, DFG and MPG (Germany); INFN (Italy); NWO (Netherlands); MNiSW and NCN (Poland); MCID/IFA (Romania); MICIU and AEI (Spain); SNSF and SER (Switzerland); NASU (Ukraine); STFC (United Kingdom); DOE NP and NSF (USA). We acknowledge the computing resources that are provided by ARDC (Australia), CBPF (Brazil), CERN, IHEP and LZU (China), IN2P3 (France), KIT and DESY (Germany), INFN (Italy), SURF (Netherlands), Polish WLCG (Poland), IFIN-HH (Romania), PIC (Spain), CSCS (Switzerland), and GridPP (United Kingdom). We are indebted to the communities behind the multiple open-source software packages

on which we depend. Individual groups or members have received support from Key Research Program of Frontier Sciences of CAS, CAS PIFI, CAS CCEPP, Fundamental Research Funds for the Central Universities, and Sci. & Tech. Program of Guangzhou (China); Minciencias (Colombia); EPLANET, Marie Skłodowska-Curie Actions, ERC and NextGenerationEU (European Union); A*MIDEX, ANR, IPhU and Labex P2IO, and Région Auvergne-Rhône-Alpes (France); Alexander-von-Humboldt Foundation (Germany); ICSC (Italy); Severo Ochoa and María de Maeztu Units of Excellence, GVA, XuntaGal, GENCAT, InTalent-Inditex and Prog. Atracción Talento CM (Spain); SRC (Sweden); the Leverhulme Trust, the Royal Society and UKRI (United Kingdom).

References

- [1] L. Gan, B. Kubis, E. Passemar, and S. Tulin, *Precision tests of fundamental physics with η and η' mesons*, Phys. Rept. **945** (2022) 1, [arXiv:2007.00664](https://arxiv.org/abs/2007.00664).
- [2] C. Amsler, *The Quark structure of hadrons: an introduction to the phenomenology and spectroscopy*, vol. 949, Springer, Cham, 2018.
- [3] S. Scherer and M. R. Schindler, *Quantum chromodynamics and chiral symmetry: a primer for chiral perturbation theory*, vol. 830, Springer, Berlin, Heidelberg, 2011.
- [4] T. Feldmann, *Quark structure of pseudoscalar mesons*, Int. J. Mod. Phys. **A15** (2000) 159, [arXiv:hep-ph/9907491](https://arxiv.org/abs/hep-ph/9907491).
- [5] X.-K. Guo, Z.-H. Guo, J. A. Oller, and J. J. Sanz-Cillero, *Scrutinizing the η - η' mixing, masses and pseudoscalar decay constants in the framework of $U(3)$ chiral effective field theory*, JHEP **06** (2015) 175, [arXiv:1503.02248](https://arxiv.org/abs/1503.02248).
- [6] P. Bickert, P. Masjuan, and S. Scherer, *η - η' mixing in large- N_c chiral perturbation theory*, Phys. Rev. **D95** (2017) 054023, [arXiv:1612.05473](https://arxiv.org/abs/1612.05473).
- [7] T. Feldmann, P. Kroll, and B. Stech, *Mixing and decay constants of pseudoscalar mesons*, Phys. Rev. **D58** (1998) 114006, [arXiv:hep-ph/9812269](https://arxiv.org/abs/hep-ph/9812269).
- [8] E. Kou, *On the η' gluonic admixture*, Phys. Rev. **D63** (2001) 054027, [arXiv:hep-ph/9908214](https://arxiv.org/abs/hep-ph/9908214).
- [9] C. E. Thomas, *Composition of the pseudoscalar η and η' mesons*, JHEP **10** (2007) 026, [arXiv:0705.1500](https://arxiv.org/abs/0705.1500).
- [10] LHCb collaboration, R. Aaij *et al.*, *Study of η - η' mixing from measurement of $B_{(s)}^0 \rightarrow J/\psi \eta^{(\prime)}$ decay rates*, JHEP **01** (2015) 024, [arXiv:1411.0943](https://arxiv.org/abs/1411.0943).
- [11] G. S. Bali *et al.*, *Masses and decay constants of the η and η' mesons from lattice QCD*, JHEP **08** (2021) 137, [arXiv:2106.05398](https://arxiv.org/abs/2106.05398).
- [12] CSSM/QCDSF/UKQCD collaborations, Z. R. Kordov *et al.*, *State mixing and masses of the π^0 , η and η' mesons from $n_f = 1 + 1 + 1$ lattice QCD + QED*, Phys. Rev. **D104** (2021) 114514, [arXiv:2110.11533](https://arxiv.org/abs/2110.11533).

- [13] ETM collaboration, K. Ott nad and C. Urbach, *Flavor-singlet meson decay constants from $N_f = 2 + 1 + 1$ twisted mass lattice QCD*, *Phys. Rev.* **D97** (2018) 054508, [arXiv:1710.07986](https://arxiv.org/abs/1710.07986).
- [14] R. Escribano and E. Royo, π^0 - η - η' mixing from $V \rightarrow P\gamma$ and $P \rightarrow V\gamma$ decays, *Phys. Lett.* **B807** (2020) 135534, [arXiv:2003.08379](https://arxiv.org/abs/2003.08379).
- [15] V. Mathieu, N. Kochelev, and V. Vicente, *The physics of glueballs*, *Int. J. of Mod. Phys.* **E18** (2009) 1, [arXiv:0810.4453](https://arxiv.org/abs/0810.4453).
- [16] S. L. Adler, *Axial-vector vertex in spinor electrodynamics*, *Phys. Rev.* **177** (1969) 2426.
- [17] J. S. Bell and R. Jackiw, *A PCAC puzzle: $\pi^0 \rightarrow \gamma\gamma$ in the σ -model*, *Nuovo Cim.* **A60** (1969) 47.
- [18] W. Greiner, S. Schramm, and E. Stein, *Quantum Chromodynamics*, Springer, Berlin, Heidelberg, 2007.
- [19] D. Atwood and A. Soni, $B \rightarrow \eta' + X$ and the QCD anomaly, *Phys. Lett.* **B405** (1997) 150, [arXiv:hep-ph/9704357](https://arxiv.org/abs/hep-ph/9704357).
- [20] P. Ball, J. M. Frere, and M. Tytgat, *Phenomenological evidence for the gluon content of η and η'* , *Phys. Lett.* **B365** (1996) 367, [arXiv:hep-ph/9508359](https://arxiv.org/abs/hep-ph/9508359).
- [21] P. Zhang, L.-P. Zou, and Y. M. Cho, *Abelian decomposition and glueball-quarkonium mixing in QCD*, *Phys. Rev.* **D98** (2018) 096015, [arXiv:1606.02374](https://arxiv.org/abs/1606.02374).
- [22] C. Di Donato, G. Ricciardi, and I. Bigi, η - η' mixing: from electromagnetic transitions to weak decays of charm and beauty hadrons, *Phys. Rev.* **D85** (2012) 013016, [arXiv:1105.3557](https://arxiv.org/abs/1105.3557).
- [23] R. Fleischer *et al.*, *Exploring CP violation and η - η' mixing with the $B_{s,d}^0 \rightarrow J/\psi \eta^{(\prime)}$ systems*, *Eur. Phys. J.* **C71** (2011) 1798, [arXiv:1110.5490](https://arxiv.org/abs/1110.5490).
- [24] H.-Y. Cheng, H.-n. Li, and K.-F. Liu, *Pseudoscalar glueball mass from η - η' - G mixing*, *Phys. Rev.* **D79** (2009) 014024, [arXiv:0811.2577](https://arxiv.org/abs/0811.2577).
- [25] R. Escribano and J. Nadal, *On the gluon content of the η and η' mesons*, *JHEP* **07** (2007) 006, [arXiv:hep-ph/0703187](https://arxiv.org/abs/hep-ph/0703187).
- [26] R. Escribano, $J/\psi \rightarrow VP$ decays and the quark and gluon content of the η and η' , *Eur. Phys. J.* **C65** (2009) 467, [arXiv:0807.4201](https://arxiv.org/abs/0807.4201).
- [27] X. Liu, H.-n. Li, and Z.-J. Xiao, *Implications on η - η' -glueball mixing from $B_{d/s} \rightarrow J/\psi \eta^{(\prime)}$ decays*, *Phys. Rev.* **D86** (2012) 011501, [arXiv:1205.1214](https://arxiv.org/abs/1205.1214).
- [28] F. Ambrosino *et al.*, *A global fit to determine the pseudoscalar mixing angle and the gluonium content of the η' meson*, *JHEP* **07** (2009) 105, [arXiv:0906.3819](https://arxiv.org/abs/0906.3819).
- [29] A. Datta, H.-J. Lipkin, and P.-J. O'Donnell, *Simple relations for two body B decays to charmonium and tests for η - η' mixing*, *Phys. Lett.* **B529** (2002) 93, [arXiv:hep-ph/0111336](https://arxiv.org/abs/hep-ph/0111336).

- [30] Belle collaboration, J. Li *et al.*, *First observation of $B_s^0 \rightarrow J/\psi\eta$ and $B_s^0 \rightarrow J/\psi\eta'$* , *Phys. Rev. Lett.* **108** (2012) 181808, [arXiv:1202.0103](https://arxiv.org/abs/1202.0103).
- [31] Belle collaboration, M.-C. Chang *et al.*, *Measurement of $B^0 \rightarrow J/\psi\eta^{(\prime)}$ and constraint on the η - η' mixing angle*, *Phys. Rev. D* **85** (2012) 091102, [arXiv:1203.3399](https://arxiv.org/abs/1203.3399).
- [32] LHCb collaboration, R. Aaij *et al.*, *Evidence for the decay $B^0 \rightarrow J/\psi\omega$ and measurement of the relative branching fractions of B_s^0 meson decays to $J/\psi\eta$ and $J/\psi\eta'$* , *Nucl. Phys. B* **867** (2013) 547, [arXiv:1210.2631](https://arxiv.org/abs/1210.2631).
- [33] A. A. Alves Jr. *et al.*, *Performance of the LHCb muon system*, *JINST* **8** (2013) P02022, [arXiv:1211.1346](https://arxiv.org/abs/1211.1346).
- [34] LHCb collaboration, R. Aaij *et al.*, *LHCb detector performance*, *Int. J. Mod. Phys. A* **30** (2015) 1530022, [arXiv:1412.6352](https://arxiv.org/abs/1412.6352).
- [35] C. Abellán Beteta *et al.*, *Calibration and performance of the LHCb calorimeters in Run 1 and 2 at the LHC*, [arXiv:2008.11556](https://arxiv.org/abs/2008.11556).
- [36] R. Aaij *et al.*, *Design and performance of the LHCb trigger and full real-time reconstruction in Run 2 of the LHC*, *JINST* **14** (2019) P04013, [arXiv:1812.10790](https://arxiv.org/abs/1812.10790).
- [37] G. Dujany and B. Storaci, *Real-time alignment and calibration of the LHCb Detector in Run II*, *J. Phys. Conf. Ser.* **664** (2015) 082010.
- [38] T. Sjöstrand, S. Mrenna, and P. Skands, *PYTHIA 6.4 physics and manual*, *JHEP* **05** (2006) 026, [arXiv:hep-ph/0603175](https://arxiv.org/abs/hep-ph/0603175); T. Sjöstrand, S. Mrenna, and P. Skands, *A brief introduction to PYTHIA 8.1*, *Comput. Phys. Commun.* **178** (2008) 852, [arXiv:0710.3820](https://arxiv.org/abs/0710.3820).
- [39] I. Belyaev *et al.*, *Handling of the generation of primary events in Gauss, the LHCb simulation framework*, *J. Phys. Conf. Ser.* **331** (2011) 032047.
- [40] D. J. Lange, *The EvtGen particle decay simulation package*, *Nucl. Instrum. Meth. A* **462** (2001) 152.
- [41] N. Davidson, T. Przedzinski, and Z. Was, *PHOTOS interface in C++: Technical and physics documentation*, *Comp. Phys. Comm.* **199** (2016) 86, [arXiv:1011.0937](https://arxiv.org/abs/1011.0937).
- [42] Geant4 collaboration, J. Allison *et al.*, *Geant4 developments and applications*, *IEEE Trans. Nucl. Sci.* **53** (2006) 270; Geant4 collaboration, S. Agostinelli *et al.*, *Geant4: A simulation toolkit*, *Nucl. Instrum. Meth. A* **506** (2003) 250.
- [43] M. Clemencic *et al.*, *The LHCb simulation application, Gauss: Design, evolution and experience*, *J. Phys. Conf. Ser.* **331** (2011) 032023.
- [44] D. Müller, M. Clemencic, G. Corti, and M. Gersabeck, *ReDecay: A novel approach to speed up the simulation at LHCb*, *Eur. Phys. J. C* **78** (2018) 1009, [arXiv:1810.10362](https://arxiv.org/abs/1810.10362).
- [45] Particle Data Group, S. Navas *et al.*, *Review of particle physics*, *Phys. Rev. D* **110** (2024) 030001.

- [46] W. D. Hulsbergen, *Decay chain fitting with a Kalman filter*, Nucl. Instrum. Meth. **A552** (2005) 566, [arXiv:physics/0503191](https://arxiv.org/abs/physics/0503191).
- [47] L. Breiman, J. H. Friedman, R. A. Olshen, and C. J. Stone, *Classification and regression trees*, Wadsworth international group, Belmont, California, USA, 1984.
- [48] Y. Freund and R. E. Schapire, *A decision-theoretic generalization of on-line learning and an application to boosting*, J. Comput. Syst. Sci. **55** (1997) 119.
- [49] H. Voss, A. Hoecker, J. Stelzer, and F. Tegenfeldt, *TMVA - Toolkit for Multivariate Data Analysis with ROOT*, PoS **ACAT** (2007) 040.
- [50] LHCb collaboration, R. Aaij *et al.*, *Updated measurement of time-dependent CP-violating observables in $B_s^0 \rightarrow J/\psi K^+ K^-$ decays*, Eur. Phys. J. **C79** (2019) 706, Erratum *ibid.* **C80** (2020) 601, [arXiv:1906.08356](https://arxiv.org/abs/1906.08356).
- [51] LHCb collaboration, R. Aaij *et al.*, *Precise measurement of the f_s/f_d ratio of fragmentation fractions and of B_s^0 decay branching fractions*, Phys. Rev. **D104** (2021) 032005, [arXiv:2103.06810](https://arxiv.org/abs/2103.06810).
- [52] LHCb collaboration, R. Aaij *et al.*, *Search for the rare decay $B^0 \rightarrow J/\psi \phi$* , Chin. Phys. **C45** (2021) 043001, [arXiv:2011.06847](https://arxiv.org/abs/2011.06847).
- [53] M. Albaladejo *et al.*, *How to employ $\bar{B}^0 \rightarrow J/\psi (\pi\eta, \bar{K}K)$ decays to extract information on $\pi\eta$ scattering*, JHEP **04** (2017) 010, [arXiv:1611.03502](https://arxiv.org/abs/1611.03502).
- [54] W.-H. Liang and E. Oset, *B^0 and B_s^0 decays into $J/\psi f_0(980)$ and $J/\psi f_0(500)$ and the nature of the scalar resonances*, Phys. Lett. **B737** (2014) 70, [arXiv:1406.7228](https://arxiv.org/abs/1406.7228).
- [55] W.-H. Liang, J.-J. Xie, and E. Oset, *\bar{B}^0 , B^+ and \bar{B}_s^0 decays into J/ψ and $K\bar{K}$ or $\pi\eta$* , Eur. Phys. J. **C75** (2015) 609, [arXiv:1510.03175](https://arxiv.org/abs/1510.03175).
- [56] J. T. Li *et al.*, *The $\bar{B}_s^0 \rightarrow J/\psi \pi^0 \eta$ decay and the $a_0(980)$ - $f_0(980)$ mixing*, Chin. Phys. **C46** (2022) 083108, [arXiv:2203.13786](https://arxiv.org/abs/2203.13786).
- [57] CKMfitter group, J. Charles *et al.*, *CKMfitter global fit results as of Spring 2021*, results and plots available at <http://ckmfitter.in2p3.fr/>.
- [58] S. S. Wilks, *The large-sample distribution of the likelihood ratio for testing composite hypotheses*, Ann. Math. Stat. **9** (1938) 60.

- I. Nasteva³ [ID](#), M. Needham⁵⁹ [ID](#), E. Nekrasova⁴⁴ [ID](#), N. Neri^{30,n} [ID](#), S. Neubert¹⁸ [ID](#),
 N. Neufeld⁴⁹ [ID](#), P. Neustroev⁴⁴ [ID](#), J. Nicolini⁴⁹ [ID](#), D. Nicotra⁸² [ID](#), E.M. Niel¹⁵ [ID](#), N. Nikitin⁴⁴ [ID](#),
 L. Nisi¹⁹ [ID](#), Q. Niu⁷⁴ [ID](#), P. Nogarolli³ [ID](#), P. Nogga¹⁸ [ID](#), C. Normand⁵⁵ [ID](#),
 J. Novoa Fernandez⁴⁷ [ID](#), G. Nowak⁶⁶ [ID](#), C. Nunez⁸⁷ [ID](#), H. N. Nur⁶⁰ [ID](#),
 A. Oblakowska-Mucha⁴⁰ [ID](#), V. Obraztsov⁴⁴ [ID](#), T. Oeser¹⁷ [ID](#), A. Okhotnikov⁴⁴,
 O. Okhrimenko⁵³ [ID](#), R. Oldeman^{32,k} [ID](#), F. Oliva^{59,49} [ID](#), E. Olivart Pino⁴⁵ [ID](#), M. Olocco¹⁹ [ID](#),
 C.J.G. Onderwater⁸² [ID](#), R.H. O'Neil⁴⁹ [ID](#), J.S. Ordóñez Soto¹¹ [ID](#), D. Osthus¹⁹ [ID](#),
 J.M. Otalora Goicochea³ [ID](#), P. Owen⁵¹ [ID](#), A. Oyanguren⁴⁸ [ID](#), O. Ozcelik⁴⁹ [ID](#), F. Paciolla^{35,w} [ID](#),
 A. Padée⁴² [ID](#), K.O. Padéken¹⁸ [ID](#), B. Pagare⁴⁷ [ID](#), T. Pajero⁴⁹ [ID](#), A. Palano²⁴ [ID](#),
 M. Palutan²⁸ [ID](#), C. Pan⁷⁵ [ID](#), X. Pan^{4,c} [ID](#), S. Panebianco¹² [ID](#), G. Panshin⁵ [ID](#),
 L. Paolucci⁶³ [ID](#), A. Papanestis⁵⁸ [ID](#), M. Pappagallo^{24,h} [ID](#), L.L. Pappalardo²⁶ [ID](#),
 C. Pappenheimer⁶⁶ [ID](#), C. Parkes⁶³ [ID](#), D. Parmar⁷⁸ [ID](#), B. Passalacqua^{26,l} [ID](#), G. Passaleva²⁷ [ID](#),
 D. Passaro^{35,s,49} [ID](#), A. Pastore²⁴ [ID](#), M. Patel⁶² [ID](#), J. Patoc⁶⁴ [ID](#), C. Patrignani^{25,j} [ID](#), A.
 Paul⁶⁹ [ID](#), C.J. Pawley⁸² [ID](#), A. Pellegrino³⁸ [ID](#), J. Peng^{5,7} [ID](#), X. Peng⁷⁴, M. Pepe Altarelli²⁸ [ID](#),
 S. Perazzini²⁵ [ID](#), D. Pereima⁴⁴ [ID](#), H. Pereira Da Costa⁶⁸ [ID](#), M. Pereira Martinez⁴⁷ [ID](#),
 A. Pereiro Castro⁴⁷ [ID](#), C. Perez⁴⁶ [ID](#), P. Perret¹¹ [ID](#), A. Perrevoort⁸¹ [ID](#), A. Perro^{49,13} [ID](#),
 M.J. Peters⁶⁶ [ID](#), K. Petridis⁵⁵ [ID](#), A. Petrolini^{29,m} [ID](#), S. Pezzulo^{29,m} [ID](#), J. P. Pfaller⁶⁶ [ID](#),
 H. Pham⁶⁹ [ID](#), L. Pica^{35,s} [ID](#), M. Piccini³⁴ [ID](#), L. Piccolo³² [ID](#), B. Pietrzyk¹⁰ [ID](#), G. Pietrzyk¹⁴ [ID](#),
 R. N. Pilato⁶¹ [ID](#), D. Pinci³⁶ [ID](#), F. Pisani⁴⁹ [ID](#), M. Pizzichemi^{31,o,49} [ID](#), V. M. Placinta⁴³ [ID](#),
 M. Plo Casasus⁴⁷ [ID](#), T. Poeschl⁴⁹ [ID](#), F. Polci¹⁶ [ID](#), M. Poli Lener²⁸ [ID](#), A. Poluektov¹³ [ID](#),
 N. Polukhina⁴⁴ [ID](#), I. Polyakov⁶³ [ID](#), E. Polycarpo³ [ID](#), S. Ponce⁴⁹ [ID](#), D. Popov^{7,49} [ID](#),
 S. Poslavskii⁴⁴ [ID](#), K. Prasanth⁵⁹ [ID](#), C. Prouve⁸⁴ [ID](#), D. Provenzano^{32,k,49} [ID](#), V. Pugatch⁵³ [ID](#),
 G. Punzi^{35,t} [ID](#), J.R. Pybus⁶⁸ [ID](#), S. Qasim⁵¹ [ID](#), Q. Q. Qian⁶ [ID](#), W. Qian⁷ [ID](#), N. Qin^{4,c} [ID](#),
 S. Qu^{4,c} [ID](#), R. Quagliani⁴⁹ [ID](#), R.I. Rabadan Trejo⁵⁷ [ID](#), R. Racz⁸⁰ [ID](#), J.H. Rademacker⁵⁵ [ID](#),
 M. Rama³⁵ [ID](#), M. Ramírez García⁸⁷ [ID](#), V. Ramos De Oliveira⁷⁰ [ID](#), M. Ramos Pernas⁵⁷ [ID](#),
 M.S. Rangel³ [ID](#), F. Ratnikov⁴⁴ [ID](#), G. Raven³⁹ [ID](#), M. Rebollo De Miguel⁴⁸ [ID](#), F. Redi^{30,i} [ID](#),
 J. Reich⁵⁵ [ID](#), F. Reiss²⁰ [ID](#), Z. Ren⁷ [ID](#), P.K. Resmi⁶⁴ [ID](#), M. Ribalda Galvez⁴⁵ [ID](#),
 R. Ribatti⁵⁰ [ID](#), G. Ricart^{15,12} [ID](#), D. Riccardi^{35,s} [ID](#), S. Ricciardi⁵⁸ [ID](#), K. Richardson⁶⁵ [ID](#),
 M. Richardson-Slipper⁵⁶ [ID](#), K. Rinnert⁶¹ [ID](#), P. Robbe^{14,49} [ID](#), G. Robertson⁶⁰ [ID](#),
 E. Rodrigues⁶¹ [ID](#), A. Rodriguez Alvarez⁴⁵ [ID](#), E. Rodriguez Fernandez⁴⁷ [ID](#),
 J.A. Rodriguez Lopez⁷⁷ [ID](#), E. Rodriguez Rodriguez⁴⁹ [ID](#), J. Roensch¹⁹ [ID](#), A. Rogachev⁴⁴ [ID](#),
 A. Rogovskiy⁵⁸ [ID](#), D.L. Rolfs¹⁹ [ID](#), P. Roloff⁴⁹ [ID](#), V. Romanovskiy⁶⁶ [ID](#), A. Romero Vidal⁴⁷ [ID](#),
 G. Romolini^{26,49} [ID](#), F. Ronchetti⁵⁰ [ID](#), T. Rong⁶ [ID](#), M. Rotondo²⁸ [ID](#), S. R. Roy²² [ID](#),
 M.S. Rudolph⁶⁹ [ID](#), M. Ruiz Diaz²² [ID](#), R.A. Ruiz Fernandez⁴⁷ [ID](#), J. Ruiz Vidal⁸² [ID](#), J.
 J. Saavedra-Arias⁹ [ID](#), J.J. Saborido Silva⁴⁷ [ID](#), S. E. R. Sacha Emile R.⁴⁹ [ID](#), N. Sagidova⁴⁴ [ID](#),
 D. Sahoo⁷⁹ [ID](#), N. Sahoo⁵⁴ [ID](#), B. Saitta^{32,k} [ID](#), M. Salomon^{31,49,o} [ID](#), I. Sanderswood⁴⁸ [ID](#),
 R. Santacesaria³⁶ [ID](#), C. Santamarina Rios⁴⁷ [ID](#), M. Santimaria²⁸ [ID](#), L. Santoro² [ID](#),
 E. Santovetti³⁷ [ID](#), A. Saputi [ID](#), D. Saranin⁴⁴ [ID](#), A. Sarnatskiy⁸¹ [ID](#), G. Sarpis⁴⁹ [ID](#),
 M. Sarpis⁸⁰ [ID](#), C. Satriano^{36,u} [ID](#), M. Saur⁷⁴ [ID](#), D. Savrina⁴⁴ [ID](#), H. Sazak¹⁷ [ID](#),
 F. Sborzacchi^{49,28} [ID](#), A. Scarabotto¹⁹ [ID](#), S. Schael¹⁷ [ID](#), S. Scherl⁶¹ [ID](#), M. Schiller²² [ID](#),
 H. Schindler⁴⁹ [ID](#), M. Schmelling²¹ [ID](#), B. Schmidt⁴⁹ [ID](#), N. Schmidt⁶⁸ [ID](#), S. Schmitt¹⁷ [ID](#),
 H. Schmitz¹⁸, O. Schneider⁵⁰ [ID](#), A. Schopper⁶² [ID](#), N. Schulte¹⁹ [ID](#), M.H. Schune¹⁴ [ID](#),
 G. Schwering¹⁷ [ID](#), B. Sciascia²⁸ [ID](#), A. Sciuccati⁴⁹ [ID](#), G. Scriven⁸² [ID](#), I. Segal⁷⁸ [ID](#),
 S. Sellam⁴⁷ [ID](#), A. Semennikov⁴⁴ [ID](#), T. Senger⁵¹ [ID](#), M. Senghi Soares³⁹ [ID](#), A. Sergi^{29,m,49} [ID](#),
 N. Serra⁵¹ [ID](#), L. Sestini²⁷ [ID](#), A. Seuthe¹⁹ [ID](#), B. Sevilla Sanjuan⁴⁶ [ID](#), Y. Shang⁶ [ID](#),
 D.M. Shangase⁸⁷ [ID](#), M. Shapkin⁴⁴ [ID](#), R. S. Sharma⁶⁹ [ID](#), I. Shchemerov⁴⁴ [ID](#), L. Shchutska⁵⁰ [ID](#),
 T. Shears⁶¹ [ID](#), L. Shekhtman⁴⁴ [ID](#), Z. Shen³⁸ [ID](#), S. Sheng^{5,7} [ID](#), V. Shevchenko⁴⁴ [ID](#), B. Shi⁷ [ID](#),
 Q. Shi⁷ [ID](#), W. S. Shi⁷³ [ID](#), Y. Shimizu¹⁴ [ID](#), E. Shmanin²⁵ [ID](#), R. Shorkin⁴⁴ [ID](#),
 J.D. Shupperd⁶⁹ [ID](#), R. Silva Coutinho⁶⁹ [ID](#), G. Simi^{33,q} [ID](#), S. Simone^{24,h} [ID](#), M. Singha⁷⁹ [ID](#),
 N. Skidmore⁵⁷ [ID](#), T. Skwarnicki⁶⁹ [ID](#), M.W. Slater⁵⁴ [ID](#), E. Smith⁶⁵ [ID](#), K. Smith⁶⁸ [ID](#),

M. Smith⁶², L. Soares Lavra⁵⁹, M.D. Sokoloff⁶⁶, F.J.P. Soler⁶⁰, A. Solomin⁵⁵, A. Solovev⁴⁴, K. Solovieva²⁰, N. S. Sommerfeld¹⁸, R. Song¹, Y. Song⁵⁰, Y. Song^{4,c}, Y. S. Song⁶, F.L. Souza De Almeida⁶⁹, B. Souza De Paula³, E. Spadaro Norella^{29,m}, E. Spedicato²⁵, J.G. Speer¹⁹, P. Spradlin⁶⁰, V. Sriskaran⁴⁹, F. Stagni⁴⁹, M. Stahl⁷⁸, S. Stahl⁴⁹, S. Stanislaus⁶⁴, M. Stefaniak⁸⁸, E.N. Stein⁴⁹, O. Steinkamp⁵¹, H. Stevens¹⁹, D. Strekalina⁴⁴, Y. Su⁷, F. Suljik⁶⁴, J. Sun³², J. Sun⁶³, L. Sun⁷⁵, D. Sundfeld², W. Sutcliffe⁵¹, V. Svintozelskyi⁴⁸, K. Swientek⁴⁰, F. Swystun⁵⁶, A. Szabelski⁴², T. Szumlak⁴⁰, Y. Tan^{4,c}, Y. Tang⁷⁵, Y. T. Tang⁷, M.D. Tat²², J. A. Teijeiro Jimenez⁴⁷, A. Terentev⁴⁴, F. Terzuoli^{35,w}, F. Teubert⁴⁹, E. Thomas⁴⁹, D.J.D. Thompson⁵⁴, A. R. Thomson-Strong⁵⁹, H. Tilquin⁶², V. Tisserand¹¹, S. T'Jampens¹⁰, M. Tobin⁵, T. T. Todorov²⁰, L. Tomassetti^{26,l}, G. Tonani³⁰, X. Tong⁶, T. Tork³⁰, D. Torres Machado², L. Toscano¹⁹, D.Y. Tou^{4,c}, C. Trippi⁴⁶, G. Tuci²², N. Tuning³⁸, L.H. Uecker²², A. Ukleja⁴⁰, D.J. Unverzagt²², A. Upadhyay⁴⁹, B. Urbach⁵⁹, A. Usachov³⁹, A. Ustyuzhanin⁴⁴, U. Uwer²², V. Vagnoni²⁵, V. Valcarce Cadenas⁴⁷, G. Valenti²⁵, N. Valls Canudas⁴⁹, J. van Eldik⁴⁹, H. Van Hecke⁶⁸, E. van Herwijnen⁶², C.B. Van Hulse^{47,z}, R. Van Laak⁵⁰, M. van Veghel³⁸, G. Vasquez⁵¹, R. Vazquez Gomez⁴⁵, P. Vazquez Regueiro⁴⁷, C. Vázquez Sierra⁸⁴, S. Vecchi²⁶, J. Velilla Serna⁴⁸, J.J. Velthuis⁵⁵, M. Veltri^{27,x}, A. Venkateswaran⁵⁰, M. Verdoglia³², M. Vesterinen⁵⁷, W. Vetens⁶⁹, D. Vico Benet⁶⁴, P. Vidrier Villalba⁴⁵, M. Vieites Diaz^{47,49}, X. Vilasis-Cardona⁴⁶, E. Vilella Figueras⁶¹, A. Villa²⁵, P. Vincent¹⁶, B. Vivacqua³, F.C. Volle⁵⁴, D. vom Bruch¹³, N. Voropaev⁴⁴, K. Vos⁸², C. Vrahas⁵⁹, J. Wagner¹⁹, J. Walsh³⁵, E.J. Walton^{1,57}, G. Wan⁶, A. Wang⁷, B. Wang⁵, C. Wang²², G. Wang⁸, H. Wang⁷⁴, J. Wang⁶, J. Wang⁵, J. Wang^{4,c}, J. Wang⁷⁵, M. Wang⁴⁹, N. W. Wang⁷, R. Wang⁵⁵, X. Wang⁸, X. Wang⁷³, X. W. Wang⁶², Y. Wang⁷⁶, Y. Wang⁶, Y. W. Wang⁷⁴, Z. Wang¹⁴, Z. Wang^{4,c}, Z. Wang³⁰, J.A. Ward⁵⁷, M. Waterlaat⁴⁹, N.K. Watson⁵⁴, D. Websdale⁶², Y. Wei⁶, J. Wendel⁸⁴, B.D.C. Westhenry⁵⁵, C. White⁵⁶, M. Whitehead⁶⁰, E. Whiter⁵⁴, A.R. Wiederhold⁶³, D. Wiedner¹⁹, M. A. Wiegertjes³⁸, C. Wild⁶⁴, G. Wilkinson^{64,49}, M.K. Wilkinson⁶⁶, M. Williams⁶⁵, M. J. Williams⁴⁹, M.R.J. Williams⁵⁹, R. Williams⁵⁶, S. Williams⁵⁵, Z. Williams⁵⁵, F.F. Wilson⁵⁸, M. Winn¹², W. Wislicki⁴², M. Witek⁴¹, L. Witola¹⁹, T. Wolf²², E. Wood⁵⁶, G. Wormser¹⁴, S.A. Wotton⁵⁶, H. Wu⁶⁹, J. Wu⁸, X. Wu⁷⁵, Y. Wu^{6,56}, Z. Wu⁷, K. Wyllie⁴⁹, S. Xian⁷³, Z. Xiang⁵, Y. Xie⁸, T. X. Xing³⁰, A. Xu^{35,s}, L. Xu^{4,c}, L. Xu^{4,c}, M. Xu⁴⁹, Z. Xu⁴⁹, Z. Xu⁷, Z. Xu⁵, K. Yang⁶², X. Yang⁶, Y. Yang¹⁵, Z. Yang⁶, V. Yeroshenko¹⁴, H. Yeung⁶³, H. Yin⁸, X. Yin⁷, C. Y. Yu⁶, J. Yu⁷², X. Yuan⁵, Y Yuan^{5,7}, E. Zaffaroni⁵⁰, J. A. Zamora Saa⁷¹, M. Zavertyaev²¹, M. Zdybal⁴¹, F. Zenesini²⁵, C. Zeng^{5,7}, M. Zeng^{4,c}, C. Zhang⁶, D. Zhang⁸, J. Zhang⁷, L. Zhang^{4,c}, R. Zhang⁸, S. Zhang⁷², S. Zhang⁶⁴, Y. Zhang⁶, Y. Z. Zhang^{4,c}, Z. Zhang^{4,c}, Y. Zhao²², A. Zhelezov²², S. Z. Zheng⁶, X. Z. Zheng^{4,c}, Y. Zheng⁷, T. Zhou⁶, X. Zhou⁸, Y. Zhou⁷, V. Zhovkovska⁵⁷, L. Z. Zhu⁷, X. Zhu^{4,c}, X. Zhu⁸, Y. Zhu¹⁷, V. Zhukov¹⁷, J. Zhuo⁴⁸, Q. Zou^{5,7}, D. Zuliani^{33,q}, G. Zunica⁵⁰.

¹School of Physics and Astronomy, Monash University, Melbourne, Australia

²Centro Brasileiro de Pesquisas Físicas (CBPF), Rio de Janeiro, Brazil

³Universidade Federal do Rio de Janeiro (UFRJ), Rio de Janeiro, Brazil

⁴Department of Engineering Physics, Tsinghua University, Beijing, China

⁵Institute Of High Energy Physics (IHEP), Beijing, China

⁶School of Physics State Key Laboratory of Nuclear Physics and Technology, Peking University, Beijing, China

- ⁷University of Chinese Academy of Sciences, Beijing, China
⁸Institute of Particle Physics, Central China Normal University, Wuhan, Hubei, China
⁹Consejo Nacional de Rectores (CONARE), San Jose, Costa Rica
¹⁰Université Savoie Mont Blanc, CNRS, IN2P3-LAPP, Annecy, France
¹¹Université Clermont Auvergne, CNRS/IN2P3, LPC, Clermont-Ferrand, France
¹²Université Paris-Saclay, Centre d'Etudes de Saclay (CEA), IRFU, Saclay, France, Gif-Sur-Yvette, France
¹³Aix Marseille Univ, CNRS/IN2P3, CPPM, Marseille, France
¹⁴Université Paris-Saclay, CNRS/IN2P3, IJCLab, Orsay, France
¹⁵Laboratoire Leprince-Ringuet, CNRS/IN2P3, Ecole Polytechnique, Institut Polytechnique de Paris, Palaiseau, France
¹⁶LPNHE, Sorbonne Université, Paris Diderot Sorbonne Paris Cité, CNRS/IN2P3, Paris, France
¹⁷I. Physikalisches Institut, RWTH Aachen University, Aachen, Germany
¹⁸Universität Bonn - Helmholtz-Institut für Strahlen und Kernphysik, Bonn, Germany
¹⁹Fakultät Physik, Technische Universität Dortmund, Dortmund, Germany
²⁰Physikalischs Institut, Albert-Ludwigs-Universität Freiburg, Freiburg, Germany
²¹Max-Planck-Institut für Kernphysik (MPIK), Heidelberg, Germany
²²Physikalischs Institut, Ruprecht-Karls-Universität Heidelberg, Heidelberg, Germany
²³School of Physics, University College Dublin, Dublin, Ireland
²⁴INFN Sezione di Bari, Bari, Italy
²⁵INFN Sezione di Bologna, Bologna, Italy
²⁶INFN Sezione di Ferrara, Ferrara, Italy
²⁷INFN Sezione di Firenze, Firenze, Italy
²⁸INFN Laboratori Nazionali di Frascati, Frascati, Italy
²⁹INFN Sezione di Genova, Genova, Italy
³⁰INFN Sezione di Milano, Milano, Italy
³¹INFN Sezione di Milano-Bicocca, Milano, Italy
³²INFN Sezione di Cagliari, Monserrato, Italy
³³INFN Sezione di Padova, Padova, Italy
³⁴INFN Sezione di Perugia, Perugia, Italy
³⁵INFN Sezione di Pisa, Pisa, Italy
³⁶INFN Sezione di Roma La Sapienza, Roma, Italy
³⁷INFN Sezione di Roma Tor Vergata, Roma, Italy
³⁸Nikhef National Institute for Subatomic Physics, Amsterdam, Netherlands
³⁹Nikhef National Institute for Subatomic Physics and VU University Amsterdam, Amsterdam, Netherlands
⁴⁰AGH - University of Krakow, Faculty of Physics and Applied Computer Science, Kraków, Poland
⁴¹Henryk Niewodniczanski Institute of Nuclear Physics Polish Academy of Sciences, Kraków, Poland
⁴²National Center for Nuclear Research (NCBJ), Warsaw, Poland
⁴³Horia Hulubei National Institute of Physics and Nuclear Engineering, Bucharest-Magurele, Romania
⁴⁴Authors affiliated with an institute formerly covered by a cooperation agreement with CERN.
⁴⁵ICCUB, Universitat de Barcelona, Barcelona, Spain
⁴⁶La Salle, Universitat Ramon Llull, Barcelona, Spain
⁴⁷Instituto Galego de Física de Altas Enerxías (IGFAE), Universidade de Santiago de Compostela, Santiago de Compostela, Spain
⁴⁸Instituto de Fisica Corpuscular, Centro Mixto Universidad de Valencia - CSIC, Valencia, Spain
⁴⁹European Organization for Nuclear Research (CERN), Geneva, Switzerland
⁵⁰Institute of Physics, Ecole Polytechnique Fédérale de Lausanne (EPFL), Lausanne, Switzerland
⁵¹Physik-Institut, Universität Zürich, Zürich, Switzerland
⁵²NSC Kharkiv Institute of Physics and Technology (NSC KIPT), Kharkiv, Ukraine
⁵³Institute for Nuclear Research of the National Academy of Sciences (KINR), Kyiv, Ukraine
⁵⁴School of Physics and Astronomy, University of Birmingham, Birmingham, United Kingdom
⁵⁵H.H. Wills Physics Laboratory, University of Bristol, Bristol, United Kingdom
⁵⁶Cavendish Laboratory, University of Cambridge, Cambridge, United Kingdom
⁵⁷Department of Physics, University of Warwick, Coventry, United Kingdom
⁵⁸STFC Rutherford Appleton Laboratory, Didcot, United Kingdom

- ⁵⁹School of Physics and Astronomy, University of Edinburgh, Edinburgh, United Kingdom
⁶⁰School of Physics and Astronomy, University of Glasgow, Glasgow, United Kingdom
⁶¹Oliver Lodge Laboratory, University of Liverpool, Liverpool, United Kingdom
⁶²Imperial College London, London, United Kingdom
⁶³Department of Physics and Astronomy, University of Manchester, Manchester, United Kingdom
⁶⁴Department of Physics, University of Oxford, Oxford, United Kingdom
⁶⁵Massachusetts Institute of Technology, Cambridge, MA, United States
⁶⁶University of Cincinnati, Cincinnati, OH, United States
⁶⁷University of Maryland, College Park, MD, United States
⁶⁸Los Alamos National Laboratory (LANL), Los Alamos, NM, United States
⁶⁹Syracuse University, Syracuse, NY, United States
⁷⁰Pontifícia Universidade Católica do Rio de Janeiro (PUC-Rio), Rio de Janeiro, Brazil, associated to ³
⁷¹Universidad Andres Bello, Santiago, Chile, associated to ⁵¹
⁷²School of Physics and Electronics, Hunan University, Changsha City, China, associated to ⁸
⁷³Guangdong Provincial Key Laboratory of Nuclear Science, Guangdong-Hong Kong Joint Laboratory of Quantum Matter, Institute of Quantum Matter, South China Normal University, Guangzhou, China, associated to ⁴
⁷⁴Lanzhou University, Lanzhou, China, associated to ⁵
⁷⁵School of Physics and Technology, Wuhan University, Wuhan, China, associated to ⁴
⁷⁶Henan Normal University, Xinxiang, China, associated to ⁸
⁷⁷Departamento de Fisica , Universidad Nacional de Colombia, Bogota, Colombia, associated to ¹⁶
⁷⁸Ruhr Universitaet Bochum, Fakultaet f. Physik und Astronomie, Bochum, Germany, associated to ¹⁹
⁷⁹Eotvos Lorand University, Budapest, Hungary, associated to ⁴⁹
⁸⁰Faculty of Physics, Vilnius University, Vilnius, Lithuania, associated to ²⁰
⁸¹Van Swinderen Institute, University of Groningen, Groningen, Netherlands, associated to ³⁸
⁸²Universiteit Maastricht, Maastricht, Netherlands, associated to ³⁸
⁸³Tadeusz Kosciuszko Cracow University of Technology, Cracow, Poland, associated to ⁴¹
⁸⁴Universidade da Coruña, A Coruña, Spain, associated to ⁴⁶
⁸⁵Department of Physics and Astronomy, Uppsala University, Uppsala, Sweden, associated to ⁶⁰
⁸⁶Taras Shevchenko University of Kyiv, Faculty of Physics, Kyiv, Ukraine, associated to ¹⁴
⁸⁷University of Michigan, Ann Arbor, MI, United States, associated to ⁶⁹
⁸⁸Ohio State University, Columbus, United States, associated to ⁶⁸

^aCentro Federal de Educacão Tecnológica Celso Suckow da Fonseca, Rio De Janeiro, Brazil

^bDepartment of Physics and Astronomy, University of Victoria, Victoria, Canada

^cCenter for High Energy Physics, Tsinghua University, Beijing, China

^dHangzhou Institute for Advanced Study, UCAS, Hangzhou, China

^eLIP6, Sorbonne Université, Paris, France

^fLamarr Institute for Machine Learning and Artificial Intelligence, Dortmund, Germany

^gUniversidad Nacional Autónoma de Honduras, Tegucigalpa, Honduras

^hUniversità di Bari, Bari, Italy

ⁱUniversità di Bergamo, Bergamo, Italy

^jUniversità di Bologna, Bologna, Italy

^kUniversità di Cagliari, Cagliari, Italy

^lUniversità di Ferrara, Ferrara, Italy

^mUniversità di Genova, Genova, Italy

ⁿUniversità degli Studi di Milano, Milano, Italy

^oUniversità degli Studi di Milano-Bicocca, Milano, Italy

^pUniversità di Modena e Reggio Emilia, Modena, Italy

^qUniversità di Padova, Padova, Italy

^rUniversità di Perugia, Perugia, Italy

^sScuola Normale Superiore, Pisa, Italy

^tUniversità di Pisa, Pisa, Italy

^uUniversità della Basilicata, Potenza, Italy

^vUniversità di Roma Tor Vergata, Roma, Italy

^wUniversità di Siena, Siena, Italy

^xUniversità di Urbino, Urbino, Italy

^y Universidad de Ingeniería y Tecnología (UTEC), Lima, Peru

^z Universidad de Alcalá, Alcalá de Henares , Spain

^{aa} Facultad de Ciencias Fisicas, Madrid, Spain

[†] Deceased